Ore Geology Reviews 134 (2021) 104147

Contents lists available at ScienceDirect

Ore Geology Reviews

journal homepage: www.elsevier.com/locate/oregeorev

U-Pb zircon SHRIMP dating of a protracted magmatic setting and its volcanic emplacement: Insights from the felsic volcanic rocks hosting the sulphide ore of the giant Aljustrel deposit, Iberian Pyrite Belt

João Lains Amaral [a,b,c,*], Ana Rita Solá [c], Telmo M. Bento dos Santos [a,b], Colombo C. G. Tassinari [d], João Gonçalves [e]

[a] Departamento de Geologia, Faculdade de Ciências da Universidade de Lisboa, Ed. C6, Piso 4, Campo Grande, 1749-016 Lisboa, Portugal
[b] Instituto Dom Luiz (IDL), Ed. C1, Piso 1, Campo Grande, 1749-016 Lisboa, Portugal
[c] Laboratório Nacional de Energia e Geologia (LNEG), Bairro do Zambujal, Apartado 7586-Alfragide, 2610-999 Amadora, Portugal
[d] Instituto de Geociências e Instituto de Energia e Ambiente, Universidade de São Paulo, Rua do Lago, 562, 05508-900 São Paulo, SP, Brazil
[e] Almina – Minas do Alentejo, S.A., Algares 7600-015, Aljustrel, Portugal

ARTICLE INFO

Keywords:
Iberian Pyrite Belt
VHMS deposits
Zircon U–Pb geochronology
Felsic volcanic rocks
Prolonged magmatic activity

ABSTRACT

A geochronological study using SHRIMP U-Pb analysis of zircon grains has been conducted to date felsic volcanic rocks hosting the six massive sulphide deposits of the giant Aljustrel mining district in the Iberian Pyrite Belt. A multiple method age calculation approach was used to validate and ponder calculated Concordia ages (emplacement and inherited), which included weighted average, probability density peak(s), Tuff Zirc and Unmix functions. This approach was particularly useful to interpret the wide continuous single U-Pb ages (320–405 Ma) recorded in the Aljustrel volcanic rocks.

The volcanic pile (>250 m) that hosts the Aljustrel deposits was emplaced between 359 and 353 Ma. Upper Devonian inheritance, representing subvolcanic activity, is well-represented in the volcanic rocks of Aljustrel (373–365 Ma). Older Devonian inherited zircon ages at 405 Ma, 388 Ma and 380 Ma were retrieved, hypothetically representing deep plutonism or other melting episodes, which suggests a long-lasting (~50 Ma) magmatic activity in the Aljustrel district. Older pre-Devonian inherited ages, uppermost Silurian and early to late Cambrian, and post-emplacement ages (~330–345 Ma) were also detected, with the latter reflecting Pb loss most likely driven by the main Variscan orogenic event.

Maximum ages obtained for the volcanic rocks in the different deposits open the possibility that the last pulses of volcanic activity and subsequent deposition of the massive sulphides were diachronic in the different Aljustrel sub-basins. Additionally, results imply that, contrary to previously assumed, Gavião and São João-Moinho deposits are probably not the same ore lens disrupted by tardi-Variscan faults. This opens new opportunities for mining exploration and targeting in the Aljustrel district and points out the importance of high-resolution geochronological studies in mining and brownfield areas.

1. Introduction

Volcanogenic massive sulphides (VMS) are important polymetallic commodities representing ~20% of the worldwide Cu + Zn + Pb mineral resources, with an estimated global tonnage of 4245.7 Mt averaging 4.17% (Mudd et al., 2017). In the Iberian Pyrite Belt (IPB), the current 7 mine operations have a total estimated resource tonnage of ~200–250 Mt; which represents ~10–15% of the overall ore identified and exploited in this belt (Leistel et al., 1997).

The IPB has been characterized as a world-class volcanogenic massive sulphide (VMS) or volcanic-hosted massive sulphide (VHMS) belt (Relvas et al., 2001; Tornos, 2006). VHMS ore deposits are often generated in a subaqueous rift-related environment, in which sulphides precipitate from hydrothermal fluids forming stratiform ores (and feeder ores) at seafloor or just below it, commonly hosted by felsic or bimodal volcanic-rich successions. VHMS deposits can also be found associated to detrital-rich successions in which direct evidences of volcanism may only be found in distal volcanogenic/tuffaceous layers (Hart et al., 2004;

* Corresponding author.
E-mail address: joao.lains.amaral@gmail.com (J. Lains Amaral).

https://doi.org/10.1016/j.oregeorev.2021.104147
Received 22 December 2020; Received in revised form 16 March 2021; Accepted 28 March 2021
Available online 6 April 2021

Herrington et al., 2005). In the case of the IPB, the variety of host rocks lead Tornos (2006) and Oliveira et al. (2019) to divide the IPB deposits into two main types: (1) shale-related massive sulphides, where massive and stockwork ore is mostly hosted by shales (e.g. Tharsis deposits); and (2) felsic volcanic-hosted massive sulphides, where massive and stockwork ore is mostly hosted by volcanic rocks (e.g. Aljustrel and Rio Tinto deposits).

Recent studies have dated the overall sequence of the IPB at different locations, and particularly for our purpose, have constrained the age of sulphide hosting rocks. Palynostratigraphic studies have successfully dated the stratiform massive ore bodies that are interlayered or interfingered with black shales (e.g. González et al., 2002; Oliveira et al., 2004). On the other hand, U-Pb zircon geochronological studies have constrained in detail the age of the volcanic rocks associated with the ore bodies (Barrie et al., 2002; Donaire et al., 2020; Dunning et al., 2002; Nesbitt et al., 1999; Oliveira et al., 2013; Paslawski et al., 2020; Pereira et al., 2014; Rosa et al., 2008, 2009; Solá et al., 2015; Valenzuela et al., 2011). In addition, direct ages of the ore have been obtained using several radiometric methods (Li et al., 2019; Mathur et al., 1999; Munhá et al., 2005; Nieto et al., 1999; Relvas et al., 2001). The overall consistency of the used methods sets up the deposition of massive sulphide lenses to have occurred between the Upper Devonian and lower Mississippian. Recently, a southwest to northeast age trend, from older to younger, of the volcanic episodes have been suggested by several authors (Barrie et al., 2002; Rosa et al., 2009; Oliveira et al., 2019 and references therein). However, the presence of older Devonian inherited zircons, points out that magmatic activity in some IPB sectors may have been active for 30–60 Ma (Oliveira et al., 2013; Rosa et al., 2009; Solá et al., 2015), implying a much more complex thermal history and magmatogenesis prior to the formation of massive sulphides and prior and/or contemporaneous to the deposition of the oldest known rocks of the IPB. Inherited zircons in magmatic rocks are, thus, a key tool to unfold the unexposed continental crust basement of the IPB (e.g. Braid et al., 2012).

In this work, we focused on the felsic volcanic rocks hosting the economic mineralization of the Aljustrel Mine and near-mining Gavião deposit: the Aljustrel district. This mining district is one of the most outstanding deposits identified in the IPB with >100 Mt of sulphides. A detailed and robust U-Pb SHRIMP zircon geochronological study of the felsic rocks hosting the mineralization of the Aljustrel district is presented. The present study aims to constrain the precipitation age of every massive sulphide ore lens at the Aljustrel district and to unfold the occurrence of early Devonian to early Carboniferous zircon populations. It is also in the scope of the present paper to provide new insights about the magmatic and geological evolution of the IPB and to provide a tool for the identification of different zircon populations in magmatic rocks rich in inherited zircons related to long-lasting magmatic settings.

2. Geological setting

The South Portuguese Zone (SPZ), with Avalonian affinities (e.g. Pereira et al., 2018), is thought to have accreted to the rest of the Iberian Massif, part of Gondwana, during the Variscan Orogeny (Oliveira et al., 2019 and references therein). The IPB is a domain of this major paleogeographic zone (Fig. 1). The lowermost group of the IPB, the Phyllite-Quartzite Group (PQG), of at least Givetian (basement is unknown) to Famennian in its uppermost section, has been interpreted to represent a passive margin setting (e.g. Braid et al., 2011; Mendes et al., 2020). This sequence is overlain by the Volcanic-Sedimentary Complex (VSC) of late Famennian to middle Visean age. The VSC, hosting the economic mineralization, has been interpreted to have formed in an extensional regime (Oliveira et al., 2019 and references therein). Overlying the IPB rocks is the Baixo Alentejo Flysch Group (BAFG) of late Visean to Serpukhovian age. The BAFG domain materializes a compressive regime (Oliveira, 1990; Rodrigues et al., 2015; Schermerhorn, 1971).

The Iberian Pyrite Belt is a large metallogenetic province with a length of 230 km and a width of 60 km containing >90 deposits and has been traditionally divided in two main sectors: the northern branch and the southern branch (Oliveira, 1990; Oliveira et al., 2019). Shale-related deposits are common in the southern branch and are associated with the first felsic volcanism event of the IPB (V1), whereas felsic volcanic-hosted deposits associated with the second volcanism event of the IPB (V2) usually occur in the northern branch (Oliveira et al., 2019; Tornos, 2006).

The Aljustrel deposit has strong similarities with the Spanish northern branch deposits (e.g. Rio Tinto). It is a felsic volcanic-hosted deposit lacking significant shale dominant levels (rarely >2 m of black shales) – deposition of massive sulphides occurred closely to the volcanic centres, thus, inhibiting slow shale deposition – and the PQG is absent. However, the entire package of volcanic rocks of Aljustrel can be related to the initial felsic volcanism event of the IPB (V1) (Oliveira et al., 2019), which is reinforced by the presence of Grandaços-type shales (corresponding to the second tectono-stratigraphic sequence of Oliveira et al., 2019), and by the presence of basaltic lavas on top of (Leitão, 2009) and within the felsic sequence (corresponding to the first mafic volcanism of Oliveira et al., 2019). In addition, a brine pool model has been suggested for the genesis of the Aljustrel massive sulphides based on sulphur isotopes and presence of sedimentary-like textures, framboidal textures and absence of replacement fronts in the massive sulphide (Barriga and Fyfe, 1988; Inverno et al., 2008; Leitão, 2009). This model is often suggested for the shale-related deposits in opposition to the replacement type of the Spanish northern branch (Tornos, 2006).

The Aljustrel deposit shares characteristics of both the northern and southern branches, highlighting the unique setting of this giant deposit. The Aljustrel district is located close, but southwards of the Pero da Vinha-Biguina thrust that materializes the boundary between the IPB northern and southern branches (Fig. 1).

2.1. Geology of the Aljustrel deposit

The Aljustrel district is composed of six massive sulphide deposits: Feitais, Estação, Algares, Moinho, São João and Gavião (Fig. 1b). The Aljustrel sequence is, from base to top, composed of the lower VSC, upper VSC and the BAFG. The PQG is absent.

The lower VSC is composed of a thick volcanic sequence of >250 m (Barriga and Fyfe, 1997) with discrete levels of black shales and with expressive levels of massive sulphides near the top and of jasper at the top of the sequence (Fig. 2). The volcanic sequence is mostly composed of felsic rocks (particularly proximal facies), but discrete mafic levels have also been observed (Leitão, 2009; Fig. 2). The lower VSC in Aljustrel has been traditionally divided in two main sequences: the Megacrystal Volcanic Unit, which is unmineralized, and the Mine Volcanic Unit hosting the economic mineralization (Andrade and Schermerhorn, 1971; Barriga and Fyfe, 1997; Leitão, 2009; Schermerhorn et al., 1987). Geochronological studies (Barrie et al., 2002; Rosa et al., 2009) attributed a lower Tournaisian age (~355 Ma) to the emplacement of the lower VSC and reported inherited Devonian, pre-Devonian and pre-Phanerozoic zircons (see Section 6).

Hydrothermal alteration and stockwork affected the volcanic rocks, which, in more intensely altered zones, can completely obliterate the volcanic textures, producing rocks such as chloritites and sericitites. According to Barriga and Fyfe (1988), the lowermost 10 m of the Paraíso Formation (see below) is also affected by hydrothermal alteration, which is in agreement with the short temporal dating gap between the upper and lower VSC sequences.

The upper VSC is composed of a shale-dominated sequence named Paraíso Formation (Schermerhorn et al., 1987). Palynostratigraphic dating attributed it to a late Tournaisian to early Visean age (Matos et al., 2010). The Paraíso formation has some similarities with the Visean hanging wall of Neves-Corvo which includes Grandaços-type siliceous shales, Brancanes-type black pyritic shales, and Purple and Green-type shales (see Oliveira et al., 2004). In the Gavião deposit, dark-

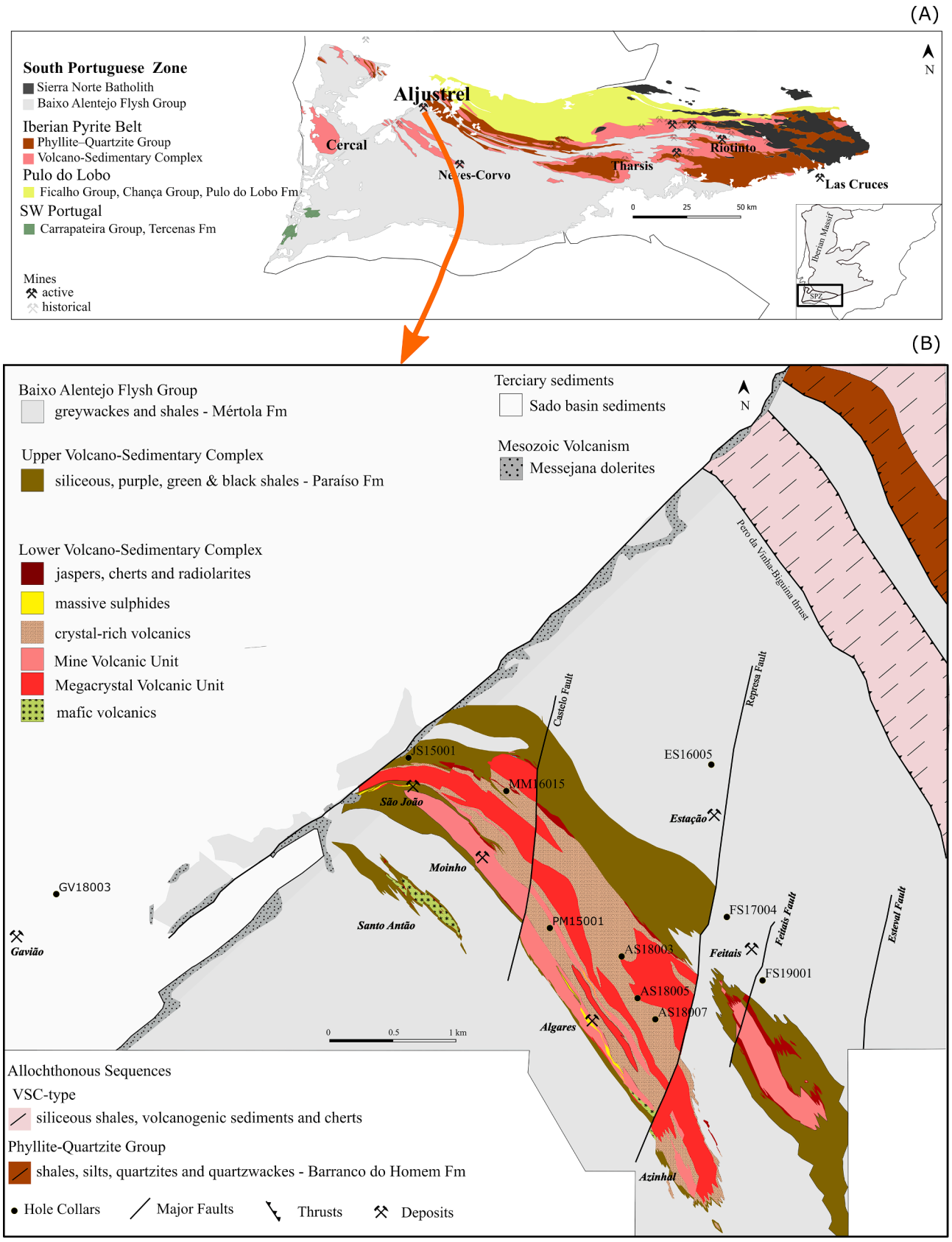

Fig. 1. a) Geological map of the South Portuguese Zone adapted from the online Iberian Geological Map (http://mapas.igme.es/gis/rest/services/Cartografia_Geologica/IGME_EP_Geologico_1M_2018/MapServer); b) Geological map of Aljustrel adapted from Schermerhorn et al. (1987) and Leitão (2009).

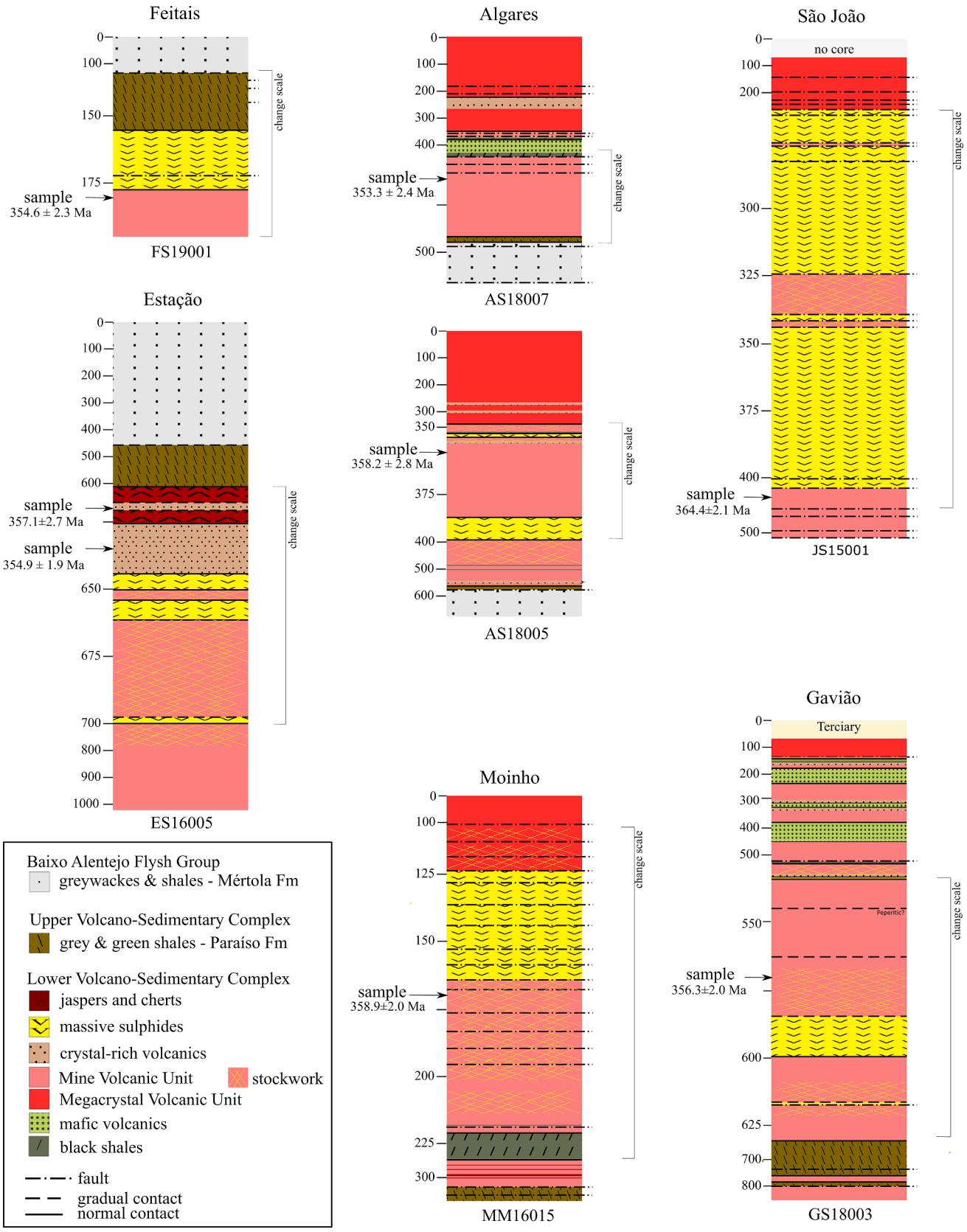

Fig. 2. Schematic drill hole logging columns of selected holes with the position of the geochronological samples (arrows). Straight lines – normal contacts, dashed lines – gradual contacts; Dash and dot line – shears and brittle faults. Location is shown in Fig. 1.

grey shales interbedded with siltstones constitute the Gavião Formation, which was only identified in drill holes and interpreted as a lateral equivalent of the Paraíso Formation (Relvas et al., 2011).

The IPB sequence in Aljustrel is overlain by the middle-late Visean turbiditic sequence (Mértola Formation of the BAFG; Matos et al., 2010), which materializes a foreland basin formed during the continental collision between the Ossa-Morena Zone and the South Portuguese Zone (Rodrigues et al., 2015).

According to Munhá (1990), Aljustrel is located along the low-grade zone, prehnite-pumpellyite facies of regional Variscan metamorphism.

The Variscan Orogeny deformed the Aljustrel sequence into 4 main structures: the Feitais Anticline, in which Feitais and Estação deposits are located; the barren Central Anticline, in which most of the Mega-crystal Volcanic Unit occurs; the São João Syncline-SW Anticline, where São João, Algares, Moinho and Gavião deposits occur; and the barren Santo Antão Anticline. Tardi- to post-orogenic N-S to NE-SW faults, including the major Messejana Fault, truncate some of those structures (Barriga and Fyfe, 1997; Relvas et al., 2011). This later deformation strongly affected Moinho and São João deposits (Fig. 2) and split Estação-Algares single massive sulphide deposit into two (Silva et al., 1997).

3. Volcanic sampling characterization

3.1. Sampling strategy

Sampling for geochronological studies was carried out in nine drill holes of the six known deposits of the Aljustrel district – Feitais, Estação, Algares, Moinho, São João and Gavião – and in one regional drill hole between Algares and Moinho deposits (Figs. 1 and 2). The sampling strategy for geochronology was mainly focused on the Mine Volcanic Unit – mostly coherent or autoclastic facies – hosting the sulphide mineralization. A sample of the barren Megacrystal Volcanic Unit was also dated for comparison. Overall, a total of 11 samples of felsic volcanic rocks were selected with the following distribution (Table 1–3; Fig. 2): (1) Feitais deposit: 2 samples of massive volcanic rocks hosting mineralization, one of the samples was collected more proximal to the massive sulphides and another more distal to it; (2) Estação deposit: 2 massive crystal-rich volcanic rocks, one of the samples was collected within jaspers and another below the jaspers and above the massive sulphides; (3) Algares deposit: 1 chloritite and 2 massive volcanic rocks hosting mineralization, one of the samples was collected more proximal to the massive sulphides and another more distal to it; (4) between Algares and Moinho deposits: 1 sample of volcanic rock, containing K-feldspar megacrystals (unmineralized Megacrystal Volcanic Unit) located in the reverse limb; (5) Moinho deposit: 1 sample of a volcanic rock hosting mineralization; (6) São João deposit: 1 sample of a sericitic volcanic rock in contact by a fault with the massive sulphides; and (7) Gavião deposit: 1 sample of a chloritite hosting mineralization.

3.2. Chemostratigraphy and physical volcanology

Previous geochemical studies, based on immobile element ratios, identified several distinct volcanic felsic rock types in Feitais deposit (Barrett, 2008; Barrett et al., 2008). The presented geochemical data (Table 1) has the sole purpose of briefly characterizing the samples that were used for the geochronological studies in order to correlate them with the chemostratigraphic groups of the lower VSC previously defined by Barrett (2008) and Barrett et al. (2008). Further geochemical inferences will be made elsewhere using a substantially larger dataset.

The 11 felsic samples plot near the boundary between rhyolite and rhyodacite/ dacite fields of Winchester and Floyd (1977). The majority of the samples are classified as rhyodacites or dacites with subordinate ones as rhyolites (Fig. 3a). All samples plot in the sub-alkaline field of Leat et al. (1986) (Fig. 3c). Fig. 3b shows that the 11 samples selected for geochronology belong to the RHY A, B, C, M and Z chemotypes of Barrett (2008) and Barrett et al. (2008).

The sericitic sample taken at São João has a RHY Z type composition. According to the unpublished report of Barrett (2008), chemotype RHY Z often relates to volcanogenic sediments that occur above RHY C associated with the Jasper and Chert Unit or above the exhalative unit at the lowermost sections of the Paraíso Formation. However, from what was observed during sample description, this sample taken from a rather massive level at São João, JS15001-407, is a coherent aphyric level that was strongly sericitized.

Of the 11 samples, 9 were classified as RHY A, B and C chemotypes, which, according to Barrett et al. (2008), are the typical rock types hosting the mineralization. The sample containing K-feldspar megacrysts was classified as RHY M, which, according to Barrett et al. (2008), is the typical rock type of the barren Megacrystal Volcanic Unit. In addition, the 11 samples were mainly interpreted as coherent to autoclastic lavas (Table 1 and 3; Fig. 4a–h).

4. Materials and methods

4.1. Sample preparation and zircon separation

Sample preparation was done at DG-FCUL - Departamento de Geologia da Faculdade de Ciências da Universidade de Lisboa, Portugal and included crushing of samples in a jaw crusher and grinding in a ring mill, followed by sieving (<250 μm fraction). A minimum of 0.5 kg was obtained for this fraction in each sample.

The separation process took place at the Campus São Mamede de Infesta of LNEG - Laboratório Nacional de Energia e Geologia, Portugal. The light minerals from the finer fractions were removed using a routine Wilfley table. Then, for pyrite-rich fractions, sulphides were leached using nitric acid (n = 8). Afterwards, the sample was separated into fractions with different magnetic susceptibilities using a Frantz Isodynamic Separator. Subsequently, methylene iodide liquid separation

Table 1
Selected geochemical whole-rock analysis of the studied rocks.

Deposit	Feitais		Estação		Algares			Step-out	Moinho	São João	Gavião
Drill hole	FS19001	FS17004	ES16005	ES16005	AS18007	AS18005	AS18003	PM15001	MM16015	JS15001	GS18003
Depth (m)	182.5	327.8	620.2	635	436	359.5	359.3	521.1	168	407	571
MgO (wt%)	4.09	0.16	3.84	4.04	2.44	1.66	24.70	0.75	3.82	2.28	27.00
Fe_2O_3T (wt%)	3.69	2.12	20.00	4.32	3.21	2.09	14.75	3.31	14.05	2.78	8.91
TiO_2 (wt%)	0.19	0.15	0.12	0.23	0.22	0.34	0.32	0.52	0.12	0.09	0.33
Al_2O_3 (wt%)	16.00	12.70	10.35	18.60	13.45	16.70	19.65	14.85	6.90	11.40	18.90
Na_2O (wt%)	1.21	4.04	2.21	1.38	2.35	2.74	<0.01	4.69	0.01	0.08	<0.01
K_2O (wt%)	1.74	3.54	0.38	2.43	3.30	1.77	<0.01	2.10	0.04	3.12	0.02
CaO (wt%)	1.59	0.28	3.38	1.42	1.24	1.74	0.47	1.05	0.12	0.27	0.75
Nb (ppm)	12.3	10.7	6.7	12.8	9.4	12.4	14.0	16.6	5.7	8.1	14.3
Zr (ppm)	284	224	124	221	243	391	347	309	143	77	364
Y (ppm)	66.3	53.2	13.4	76.5	48.1	73.7	77.6	43.0	24.2	17.8	71.4
Th (ppm)	15.95	13.80	11.45	20.40	18.35	25.30	25.20	13.65	8.98	6.00	26.4
U (ppm)	9.09	25.90	0.29	3.52	4.06	5.85	7.46	4.06	3.43	2.08	6.39

Table 2
U-Pb SHRIMP U-Pb analytical data (all errors are reported at 1σ).

Drill hole	Depth (m)	Spot n°	U (ppm)	Th (ppm)	Th/U	$^{206}Pb/^{238}U$ (Ma)	1 σ (abs)	$^{207}Pb/^{206}Pb$ (Ma)	1 σ (abs)	$^{207}Pb/^{235}U$	1 σ (%)	$^{206}Pb/^{238}U$	1 σ (%)	error corr.	$^{206}Pb_c$ (%)	disc. (%)	interpreted fraction	notes
FS19001	182.5	10.1	437.0	183.7	0.4	**340.8**	3.7	496.2	280.5	0.428	12.777	0.054	1.108	0.087	3.05	32.1	Pb loss	d >|10|%, $^{206}Pb_C$ > 1% , σ > 5%
		6.2	171.7	77.0	0.4	**342.1**	3.8	342.0	195.6	0.401	8.716	0.055	1.155	0.132	1.06	0.0	Pb loss	$^{206}Pb_C$ > 1% , σ > 5%
		4.1	139.3	81.3	0.6	**343.3**	3.8	352.9	206.7	0.404	9.219	0.055	1.123	0.122	1.19	2.8	Pb loss	$^{206}Pb_C$ > 1% , σ > 5%
		7.1	184.1	93.7	0.5	**346.9**	3.7	356.9	187.7	0.409	8.383	0.055	1.086	0.130	1.38	2.9	Pb loss	$^{206}Pb_C$ > 1% , σ > 5%
		2.1	228.9	105.0	0.5	**351.3**	3.3	390.6	81.6	0.421	3.763	0.056	0.965	0.256	0.60	10.3	emplacement	d >|10|%
		11.2	290.8	164.0	0.6	**351.7**	3.2	360.5	104.4	0.416	4.722	0.056	0.947	0.200	0.69	2.5	emplacement	
		11.1	423.4	288.8	0.7	**352.1**	3.7	358.0	73.1	0.416	3.417	0.056	1.090	0.319	0.52	1.7	emplacement	
		12.1	112.6	49.7	0.4	**352.7**	4.3	315.6	251.1	0.409	11.114	0.056	1.265	0.114	1.65	−12.1	emplacement	d >|10|%, $^{206}Pb_C$ > 1% , σ > 5%
		3.1	944.3	628.3	0.7	**352.7**	2.8	345.7	49.1	0.414	2.315	0.056	0.810	0.350	0.42	−2.1	emplacement	
		6.1	728.7	419.4	0.6	**356.3**	2.9	341.7	73.6	0.418	3.356	0.057	0.835	0.249	0.59	−4.4	emplacement	
		13.1	200.7	98.8	0.5	**356.4**	3.5	368.8	101.0	0.423	4.598	0.057	1.018	0.221	0.62	3.5	emplacement	
		8.1	210.8	117.5	0.6	**358.1**	4.7	389.5	79.5	0.429	3.791	0.057	1.353	0.357	0.54	8.3	emplacement	
		9.1	539.7	236.2	0.4	**360.0**	3.0	341.2	46.6	0.422	2.230	0.057	0.854	0.383	0.31	−5.7	emplacement	
		14.1	338.5	217.1	0.6	**366.0**	3.4	324.3	124.9	0.426	5.583	0.058	0.950	0.170	0.81	−13.2	inherited	d >|10|%
		1.1	222.6	110.4	0.5	**373.4**	3.6	337.2	112.8	0.437	5.079	0.060	0.993	0.195	0.80	−11.1	inherited	d >|10|%
FS17004	327.8	19.1	258.1	138.2	0.5	**353.9**	3.1	362.4	77.9	0.419	3.571	0.056	0.902	0.253	0.36	2.4	emplacement	
		6.1	589.4	321.4	0.5	**354.8**	2.8	357.7	28.1	0.419	1.490	0.057	0.820	0.550	0.19	0.8	emplacement	
		4.1	365.0	315.2	0.9	**355.8**	4.0	362.8	39.8	0.421	2.111	0.057	1.159	0.549	0.25	2.0	emplacement	
		8.1	419.0	365.6	0.9	**356.5**	3.0	398.4	58.8	0.428	2.766	0.057	0.879	0.318	0.71	10.8	emplacement	d >|10|%
		1.1	329.3	273.8	0.8	**358.5**	3.1	366.6	74.7	0.425	3.429	0.057	0.881	0.257	0.36	2.3	emplacement	
		2.1	400.1	367.0	0.9	**358.9**	3.0	364.6	36.6	0.425	1.838	0.057	0.859	0.467	0.22	1.6	emplacement	
		5.1	269.8	138.4	0.5	**365.6**	3.2	395.2	63.5	0.439	2.973	0.058	0.912	0.307	0.59	7.7	main inherited	
		3.1	957.8	441.1	0.5	**366.1**	2.8	335.9	27.5	0.428	1.453	0.058	0.799	0.550	0.20	−9.3	main inherited	
		7.1	985.1	382.1	0.4	**373.4**	2.9	384.1	20.1	0.447	1.198	0.060	0.796	0.665	0.17	2.9	main inherited	
		17.1	266.5	148.4	0.6	**406.1**	4.5	382.0	238.4	0.486	10.667	0.065	1.142	0.107	3.12	−6.5	inherited	$^{206}Pb_C$ > 1% , σ > 5%
		18.1	381.4	135.9	0.4	**492.1**	5.1	467.2	30.1	0.617	1.736	0.079	1.079	0.622	0.13	−5.5	pre-Devonian	

(*continued on next page*)

Table 2 (*continued*)

Drill hole	Depth (m)	Spot n°	U (ppm)	Th (ppm)	Th/U	$^{206}Pb/^{238}U$ (Ma)	1 σ (abs)	$^{207}Pb/^{206}Pb$ (Ma)	1 σ (abs)	$^{207}Pb/^{235}U$	1 σ (%)	$^{206}Pb/^{238}U$	1 σ (%)	error corr.	$^{206}Pb_c$ (%)	disc. (%)	interpreted fraction	notes
ES16005	620.2	15.1	810.4	27.1	0.0	**350.2**	4.6	365.8	183.4	0.415	8.248	0.056	1.356	0.164	2.88	4.4	emplacement	$^{206}Pb_C > 1\%$, σ > 5%
		8.1	287.7	205.9	0.7	**353.0**	3.4	386.4	143.1	0.422	6.446	0.056	0.976	0.151	1.20	8.9	emplacement	$^{206}Pb_C > 1\%$, σ > 5%
		6.1	304.7	278.8	0.9	**356.9**	3.3	362.2	75.4	0.422	3.471	0.057	0.942	0.271	0.57	1.5	emplacement	
		3.1	230.4	202.9	0.9	**358.3**	3.5	381.9	125.5	0.428	5.675	0.057	1.012	0.178	1.45	6.4	emplacement	$^{206}Pb_C > 1\%$, σ > 5%
		16.1	199.7	224.7	1.1	**359.0**	3.7	334.0	182.2	0.419	8.108	0.057	1.053	0.130	1.44	−7.7	emplacement	$^{206}Pb_C > 1\%$, σ > 5%
		4.1	308.3	360.8	1.2	**359.5**	3.3	380.7	85.4	0.429	3.913	0.057	0.932	0.238	0.59	5.7	emplacement	
		5.1	285.1	82.8	0.3	**359.9**	3.3	335.2	102.2	0.421	4.609	0.057	0.943	0.205	0.49	−7.6	emplacement	
		17.1	301.3	258.2	0.9	**364.0**	4.1	347.8	61.5	0.428	2.952	0.058	1.152	0.390	0.47	−4.8	main inherited	
		18.1	509.2	526.8	1.0	**364.1**	3.0	359.4	36.9	0.430	1.840	0.058	0.842	0.458	0.23	−1.3	main inherited	
		9.1	289.5	82.7	0.3	**364.4**	3.6	321.9	195.1	0.424	8.647	0.058	1.003	0.116	1.40	−13.6	main inherited	d >|10|%, $^{206}Pb_C > 1\%$, σ > 5%
		20.1	396.1	154.0	0.4	**364.8**	3.1	387.0	66.0	0.437	3.066	0.058	0.873	0.285	0.49	5.9	main inherited	
		12.1	493.1	423.3	0.9	**365.1**	3.2	353.0	101.3	0.430	4.576	0.058	0.904	0.197	1.27	−3.5	main inherited	$^{206}Pb_C > 1\%$
		2.1	375.8	212.1	0.6	**365.9**	3.2	362.0	87.5	0.433	3.984	0.058	0.908	0.228	0.82	−1.1	main inherited	
		11.1	262.3	83.4	0.3	**370.1**	3.6	321.8	139.4	0.430	6.217	0.059	0.998	0.160	0.87	−15.4	inherited	σ > 5%
		14.1	248.8	114.2	0.5	**370.1**	3.6	364.1	199.9	0.439	8.922	0.059	1.007	0.113	1.76	−1.7	inherited	$^{206}Pb_C > 1\%$, σ > 5%
		10.1	305.5	162.7	0.5	**370.3**	3.6	369.6	110.7	0.440	5.017	0.059	1.000	0.199	1.12	−0.2	inherited	$^{206}Pb_C > 1\%$, σ > 5%
		13.1	397.9	141.6	0.4	**380.2**	3.3	362.5	67.5	0.451	3.129	0.061	0.905	0.289	0.43	−5.0	inherited	
		19.1	473.0	134.9	0.3	**531.2**	5.2	519.6	25.8	0.684	1.551	0.086	1.012	0.653	0.18	−2.3	pre-Devonian	
ES16005	635	10.2	354.5	101.6	0.3	**330.4**	3.4	376.2	113.9	0.392	5.172	0.053	1.055	0.204	1.30	12.5	Pb loss	d >|10|%, $^{206}Pb_C > 1\%$, σ > 5%
		21.1	392.3	416.6	1.1	**334.8**	3.9	367.4	49.1	0.396	2.489	0.053	1.202	0.483	0.44	9.1	Pb loss	
		19.1	114.5	74.1	0.6	**348.3**	3.9	382.1	173.8	0.415	7.818	0.056	1.163	0.149	1.99	9.1	emplacement	$^{206}Pb_C > 1\%$, σ > 5%
		16.1	299.3	142.7	0.5	**349.1**	3.1	356.6	72.9	0.412	3.352	0.056	0.908	0.271	0.69	2.2	emplacement	
		11.1	590.4	552.2	0.9	**352.2**	2.8	352.7	28.4	0.415	1.499	0.056	0.821	0.547	0.17	0.2	emplacement	
		14.1	211.9	66.3	0.3	**352.5**	3.3	345.2	88.6	0.414	4.032	0.056	0.966	0.240	0.72	−2.1	emplacement	
		18.1b	301.8	115.2	0.4	**352.7**	3.1	361.2	49.2	0.417	2.356	0.056	0.894	0.380	0.32	2.4	emplacement	
		13.1	458.7	593.0	1.3	**354.5**	2.9	354.6	37.6	0.418	1.866	0.057	0.842	0.451	0.27	0.0	emplacement	
		23.1	219.3	52.6	0.2		3.3		62.6		2.925		0.942	0.322		−3.2	emplacement	

(*continued on next page*)

Table 2 (*continued*)

Drill hole	Depth (m)	Spot n°	U (ppm)	Th (ppm)	Th/U	$^{206}Pb/^{238}U$ (Ma)	1 σ (abs)	$^{207}Pb/^{206}Pb$ (Ma)	1 σ (abs)	$^{207}Pb/^{235}U$	1 σ (%)	$^{206}Pb/^{238}U$	1 σ (%)	error corr.	$^{206}Pb_c$ (%)	disc. (%)	interpreted fraction	notes
						355.6		345.0		0.417		0.057			0.35			
		17.1	501.6	467.5	0.9		2.9		48.7		2.315		0.842	0.364		−0.3	emplacement	
						358.6		357.4		0.423		0.057			0.28			
		12.1	291.3	124.5	0.4		3.9		229.7		10.201		1.103	0.108		−5.9	emplacement	$^{206}Pb_C > 1\%$, σ > 5%
						359.1		339.5		0.421		0.057			1.68			
		22.1	430.8	550.9	1.3		3.0		34.4		1.746		0.856	0.491		−1.9	emplacement	
						359.3		352.7		0.423		0.057			0.14			
		18.1	554.1	674.5	1.2		2.9		40.7		1.988		0.832	0.418		2.7	emplacement	
						359.9		369.7		0.427		0.057			0.42			
		15.1	251.3	85.1	0.3		3.4		89.1		4.060		0.940	0.232		−3.5	main inherited	
						370.0		357.9		0.437		0.059			0.72			
		24.1	408.1	142.6	0.3		3.1		36.6		1.838		0.859	0.467		−0.8	main inherited	
						371.6		368.6		0.441		0.059			0.24			
		25.1	306.5	100.1	0.3		3.5		95.0		4.328		0.949	0.219		0.6	main inherited	
						375.2		377.3		0.447		0.060			0.78			
		20.1	243.9	100.7	0.4		3.6		131.3		5.933		0.990	0.167		3.5	main inherited	$^{206}Pb_C > 1\%$, σ > 5%
						378.3		391.5		0.454		0.060			1.66			
AS18007	436	13.1	123.7	115.4	0.9		3.5		145.1		6.535		1.113	0.170		12.3	Pb loss	d >|10|%, $^{206}Pb_C > 1\%$, σ > 5%
						324.3		368.4		0.384		0.052			1.11			
		16.1	423.0	625.9	1.5		2.9		36.6		1.832		0.847	0.462		6.5	emplacement	
						347.6		371.2		0.413		0.055			0.30			
		1.1	154.3	134.8	0.9		3.5		102.7		4.665		1.040	0.223		1.0	emplacement	
						350.7		354.0		0.413		0.056			0.84			
		5.1	218.1	97.5	0.4		3.3		79.8		3.653		0.960	0.263		−2.9	emplacement	
						351.2		341.6		0.411		0.056			0.60			
		12.1	244.2	130.4	0.5		3.2		77.2		3.559		0.934	0.262		6.8	emplacement	
						353.9		378.7		0.422		0.056			0.86			
		15.1	1199.1	2072.7	1.7		3.0		14.7		1.094		0.877	0.802		1.5	emplacement	
						354.0		359.2		0.418		0.056			0.05			
		2.1	270.9	299.9	1.1		3.2		60.1		2.814		0.915	0.325		−0.4	emplacement	
						355.3		353.9		0.419		0.057			0.43			
		4.1	110.8	64.1	0.6		6.1		173.5		7.883		1.754	0.223		0.4	emplacement	σ > 5%
						356.5		358.0		0.421		0.057			0.71			
		9.1	393.4	369.7	0.9		3.1		51.9		2.459		0.875	0.356		−1.5	emplacement	
						359.2		354.1		0.423		0.057			0.49			
		7.1	281.5	273.7	1.0		3.3		101.7		4.620		0.933	0.202		5.0	main inherited	
						366.1		384.7		0.438		0.058			0.95			
		8.1	324.0	196.5	0.6		3.2		69.8		3.218		0.892	0.277		−2.4	main inherited	
						366.6		358.2		0.433		0.059			0.58			
		4.2	389.7	272.7	0.7		4.4		103.3		4.744		1.219	0.257		−1.2	main inherited	
						370.8		366.5		0.440		0.059			0.77			
		14.1	413.2	222.0	0.5		3.3		103.3		4.696		0.907	0.193		4.8	inherited	$^{206}Pb_C > 1\%$
						376.4		394.8		0.452		0.060			1.42			
		10.1	305.6	147.8	0.5		5.4		72.5		3.519		1.392	0.396		−3.0	inherited	
						403.8		392.4		0.486		0.065			0.24			
		6.1	499.8	266.5	0.5		3.8		60.5		2.863		0.944	0.330		−5.0	pre-Devonian	
						421.1		401.6		0.509		0.067			0.27			
		11.1	866.8	191.1	0.2		4.0		19.7		1.201		0.807	0.672		−11.4	pre-Devonian	d >|10|%
						518.8		467.7		0.652		0.084			0.04			
		3.1	750.1	103.3	0.1		4.2		20.2		1.225		0.815	0.665		−12.6	pre-Devonian	d >|10|%
						537.9		479.7		0.680		0.087			−0.03			
AS18005	359.5	13.2	183.8	111.8	0.6		3.5		119.8		5.417		1.060	0.196		8.2	Pb loss	
						334.6		363.7		0.395		0.053			0.99			

(*continued on next page*)

Table 2 (*continued*)

Drill hole	Depth (m)	Spot n°	U (ppm)	Th (ppm)	Th/U	$^{206}Pb/^{238}U$ (Ma)	1 σ (abs)	$^{207}Pb/^{206}Pb$ (Ma)	1 σ (abs)	$^{207}Pb/^{235}U$	1 σ (%)	$^{206}Pb/^{238}U$	1 σ (%)	error corr.	$^{206}Pb_c$ (%)	disc. (%)	interpreted fraction	notes
		6.1	319.9	323.4	1.0	**339.7**	2.9	415.8	45.9	0.411	2.233	0.054	0.877	0.393	0.41	18.8	Pb loss	d >|10|%
		8.1	265.2	215.5	0.8	**346.4**	3.1	339.0	57.5	0.405	2.699	0.055	0.922	0.342	0.32	−2.3	Pb loss	
		4.1	356.5	318.7	0.9	**350.1**	3.5	378.2	227.4	0.417	10.161	0.056	1.013	0.100	1.91	7.7	Pb loss	$^{206}Pb_C$ > 1% , σ > 5%
		14.1	182.8	82.7	0.5	**355.4**	3.4	356.2	96.5	0.419	4.384	0.057	0.977	0.223	0.46	0.2	emplacement	
		13.1	621.9	693.6	1.1	**356.2**	2.9	372.6	24.1	0.423	1.352	0.057	0.824	0.609	0.12	4.5	emplacement	
		15.1	316.7	134.7	0.4	**357.4**	3.1	385.0	36.8	0.427	1.862	0.057	0.882	0.474	0.22	7.4	emplacement	
		8.2	230.2	110.0	0.5	**359.3**	3.3	348.0	79.0	0.422	3.619	0.057	0.939	0.259	0.59	−3.3	emplacement	
		5.1	572.5	829.5	1.4	**361.2**	2.9	380.8	20.9	0.431	1.237	0.058	0.819	0.662	0.10	5.3	emplacement	
		10.1	1612.7	2872.0	1.8	**365.5**	3.0	402.7	11.7	0.440	1.004	0.058	0.857	0.853	0.12	9.5	main inherited	
		3.1	243.1	108.1	0.4	**365.5**	5.6	348.5	146.1	0.430	6.647	0.058	1.564	0.235	1.00	−5.0	main inherited	$^{206}Pb_C$ > 1% , σ > 5%
		7.1	853.7	468.7	0.5	**367.8**	2.9	341.5	21.8	0.431	1.253	0.059	0.803	0.641	0.01	−7.9	main inherited	
		12.1	426.6	370.3	0.9	**367.9**	3.1	389.7	36.1	0.441	1.820	0.059	0.854	0.469	0.25	5.8	main inherited	
		11.1	225.2	140.3	0.6	**370.6**	4.3	348.9	74.4	0.436	3.507	0.059	1.208	0.344	0.44	−6.4	main inherited	
		1.1	177.4	125.6	0.7	**372.6**	5.3	362.5	199.6	0.441	8.971	0.060	1.473	0.164	0.75	−2.9	main inherited	σ > 5%
		9.1	1693.8	1360.8	0.8	**374.1**	3.1	359.1	15.7	0.443	1.106	0.060	0.860	0.778	0.07	−4.3	main inherited	
		2.1	740.5	724.9	1.0	**383.4**	3.7	352.2	60.2	0.452	2.841	0.061	0.986	0.347	0.38	−9.1	inherited	
AS18003	359.3	9.2*	591.2	412.1	0.7	**279.7**	3.0	292.7	404.1	0.319	17.729	0.044	1.097	0.062	6.14	4.5	Pb loss	$^{206}Pb_c$ > 1% , σ > 5%
		10.1	239.9	188.9	0.8	**323.1**	3.6	318.4	232.1	0.374	10.274	0.051	1.138	0.111	2.68	−1.5	Pb loss	$^{206}Pb_C$ > 1% , σ > 5%
		3.1	260.6	207.1	0.8	**338.4**	3.2	375.4	136.0	0.402	6.120	0.054	0.962	0.157	1.14	10.1	Pb loss	d >|10|%, $^{206}Pb_C$ > 1% , σ > 5%
		8.1	970.7	892.8	0.9	**350.5**	3.5	324.5	55.6	0.408	2.661	0.056	1.040	0.391	0.81	−8.2	emplacement	
		6.1	239.6	105.0	0.4	**351.0**	3.4	334.4	116.1	0.410	5.215	0.056	0.984	0.189	0.65	−5.1	emplacement	
		9.1	648.7	462.8	0.7	**358.8**	2.9	301.9	57.2	0.413	2.644	0.057	0.838	0.317	0.26	−19.4	emplacement	d >|10|%
		12.1	628.6	610.2	1.0	**359.3**	3.0	321.1	42.5	0.417	2.056	0.057	0.854	0.415	0.12	−12.2	emplacement	d >|10|%
		2.1	595.2	880.9	1.5	**359.7**	2.9	322.1	45.4	0.418	2.170	0.057	0.840	0.387	0.25	−12.0	emplacement	d >|10|%
		7.1	423.8	325.3	0.8	**362.4**	3.1	342.5	70.6	0.425	3.243	0.058	0.882	0.272	0.41	−6.0	main inherited	
		11.1	493.7	591.7	1.2	**362.6**	3.0	384.0	64.0	0.433	2.975	0.058	0.857	0.288	0.33	5.7	main inherited	
		4.1	324.3	134.9	0.4	**368.9**	4.8	341.7	90.0	0.433	4.198	0.059	1.348	0.321	0.59	−8.2	main inherited	
		13.1	204.7	103.6	0.5		3.8		164.1		7.395		1.038	0.140		6.6	main inherited	$^{206}Pb_C$ > 1% , σ > 5%

(*continued on next page*)

Table 2 (*continued*)

Drill hole	Depth (m)	Spot n°	U (ppm)	Th (ppm)	Th/U	$^{206}Pb/^{238}U$ (Ma)	1 σ (abs)	$^{207}Pb/^{206}Pb$ (Ma)	1 σ (abs)	$^{207}Pb/^{235}U$	1 σ (%)	$^{206}Pb/^{238}U$	1 σ (%)	error corr.	$^{206}Pb_c$ (%)	disc. (%)	interpreted fraction	notes
						372.2		397.7		0.448		0.059			1.09			
		1.1	526.5	353.6	0.7		3.2		52.5		2.470		0.874	0.354		−19.8	inherited	d >|10|%
						382.4		320.8		0.445		0.061			0.23			
		1.2*	1428.0	1221.9	0.9	**405.1**	21.8		1051.0		47.816		5.555	0.116		14.5	inherited	d >|10|%, $^{206}Pb_C$ > 1% , σ > 5%
								471.2		0.505		0.065			19.73			
PM15001	521.3	7.1	84.2	75.1	0.9		4.8		308.9		13.717		1.464	0.107		0.3	Pb loss	$^{206}Pb_C$ > 1% , σ > 5%
						338.9		339.7		0.396		0.054			2.55			
		8.1	66.6	84.3	1.3		5.3		337.1		14.867		1.584	0.107		−13.8	Pb loss	d >|10|%, $^{206}Pb_C$ > 1% , σ > 5%
						341.4		301.0		0.393		0.054			2.56			
		1.1	133.2	83.3	0.6		3.8		169.0		7.593		1.135	0.149		7.5	emplacement	$^{206}Pb_C$ > 1% , σ > 5%
						347.8		375.0		0.414		0.055			1.27			
		6.1	206.1	41.5	0.2		3.4		88.8		4.052		1.000	0.247		−1.9	emplacement	
						350.6		344.1		0.411		0.056			0.49			
		4.1	160.6	127.1	0.8		3.7		159.5		7.158		1.072	0.150		4.4	emplacement	$^{206}Pb_C$ > 1% , σ > 5%
						352.4		368.1		0.418		0.056			1.04			
		13.1	188.2	78.4	0.4		3.5		114.0		5.181		1.019	0.197		9.3	emplacement	
						353.6		388.8		0.423		0.056			0.76			
		2.1	119.5	162.1	1.4		4.1		216.3		9.706		1.190	0.123		8.6	emplacement	$^{206}Pb_C$ > 1% , σ > 5%
						354.0		386.5		0.423		0.056			1.41			
		3.1	70.9	63.9	0.9		5.0		256.0		11.393		1.451	0.127		−5.0	emplacement	$^{206}Pb_C$ > 1% , σ > 5%
						354.8		338.2		0.415		0.057			1.64			
		5.1	441.8	96.7	0.2		3.0		63.9		2.958		0.872	0.295		−3.2	emplacement	
						358.2		347.3		0.421		0.057			0.59			
		10.1	408.7	31.1	0.1		3.2		66.7		3.122		0.901	0.289		16.2	emplacement	d >|10|%
						359.8		427.2		0.438		0.057			0.71			
		9.1	57.9	40.6	0.7		5.6		347.1		15.553		1.590	0.102		8.0	main inherited	$^{206}Pb_C$ > 1% , σ > 5%
						361.8		392.3		0.434		0.058			2.17			
		14.1*	411.6	70.1	0.2	**366.5**	4.1		276.1		12.270		1.154	0.094		−4.5	main inherited	$^{206}Pb_C$ > 1% , σ > 5%
								351.1		0.432		0.059			8.22			
		11.1	257.7	138.7	0.5		3.5		90.1		4.085		0.963	0.236		−15.3	inherited	d >|10|%
						378.9		329.8		0.443		0.061			0.46			
		12.1	585.7	167.1	0.3		3.1		43.5		2.100		0.839	0.400		−7.5	inherited	
						382.1		356.1		0.452		0.061			0.32			
MM16015	168	13.1	310.5	372.0	1.2		3.3		114.2		5.163		0.957	0.185		5.5	emplacement	
						353.0		373.1		0.419		0.056			0.98			
		5.1	204.4	82.5	0.4		3.6		143.1		6.452		1.029	0.159		7.4	emplacement	$^{206}Pb_C$ > 1% , σ > 5%
						354.9		382.4		0.423		0.057			1.40			
		8.1	401.3	166.6	0.4		4.4		72.5		3.454		1.252	0.362		2.7	emplacement	
						357.2		366.8		0.423		0.057			0.63			
		9.1	629.6	980.7	1.6		2.9		45.3		2.169		0.841	0.388		−6.1	emplacement	
						357.4		337.3		0.418		0.057			0.33			
		16.1	298.5	262.6	0.9		6.3		145.5		6.728		1.814	0.270		7.8	emplacement	$^{206}Pb_C$ > 1% , σ > 5%
						358.2		387.5		0.429		0.057			2.36			
		4.1	433.7	674.2	1.6		3.1		78.2		3.548		0.877	0.247		−15.4	emplacement	d >|10|%
						358.9		312.3		0.415		0.057			0.37			
		7.1	297.3	122.3	0.4		3.3		125.9		5.643		0.944	0.167		−4.6	emplacement	
						359.2		343.8		0.421		0.057			0.72			
		10.1	229.8	95.9	0.4		3.5		108.3		4.886		0.999	0.204		−6.5	emplacement	
						359.6		338.3		0.421		0.057			0.75			
		3.1	299.4	144.1	0.5		3.3		86.4		3.897		0.935	0.240		−22.4	emplacement	d >|10|%
						359.9		295.5		0.414		0.057			0.42			
		6.1	207.4	81.4	0.4		3.5		94.9		4.348		1.003	0.231		8.5	emplacement	
						362.0		394.4		0.435		0.058			0.66			
		12.1	309.1	307.7	1.0		3.5		88.4		4.053		0.989	0.244		4.9	emplacement	

(*continued on next page*)

Table 2 (*continued*)

Drill hole	Depth (m)	Spot n°	U (ppm)	Th (ppm)	Th/U	$^{206}Pb/^{238}U$ (Ma)	1 σ (abs)	$^{207}Pb/^{206}Pb$ (Ma)	1 σ (abs)	$^{207}Pb/^{235}U$	1 σ (%)	$^{206}Pb/^{238}U$	1 σ (%)	error corr.	$^{206}Pb_c$ (%)	disc. (%)	interpreted fraction	notes
						363.1		381.2		0.433		0.058			0.62			
		15.1	261.0	115.1	0.4		3.2		47.7		2.293		0.900	0.392		−5.1	emplacement	
						363.2		345.9		0.427		0.058			0.17			
		2.1	402.5	356.2	0.9		3.2		94.2		4.267		0.892	0.209		−4.0	main inherited	
						369.8		355.8		0.437		0.059			0.71			
		11.1	343.0	117.7	0.3		5.2		89.7		4.228		1.448	0.342		−3.7	main inherited	
						370.2		357.3		0.437		0.059			0.63			
		1.1	363.8	292.2	0.8		3.5		100.7		4.547		0.949	0.209		−12.2	inherited	d >|10|%
						382.3		341.9		0.449		0.061			0.67			
		14.1	317.5	161.1	0.5		4.2		190.6		8.460		1.102	0.130		–22.8	inherited	d >|10|%, $^{206}Pb_C$ > 1% , σ > 5%
						390.2		319.6		0.454		0.062			1.48			
JS15001	407	2.1	189.5	1072.0	5.7		3.4		110.8		4.993		0.973	0.195		−3.9	main inherited	
						358.2		345.0		0.420		0.057			0.67			
		11.1	257.4	678.7	2.6		4.4		71.2		3.403		1.263	0.371		3.4	main inherited	
						359.1		371.4		0.427		0.057			0.41			
		12.1	338.9	731.6	2.2		3.2		68.9		3.192		0.907	0.284		4.4	main inherited	
						360.4		376.4		0.429		0.057			0.51			
		8.1	267.8	688.4	2.6		4.0		75.4		3.537		1.127	0.319		4.1	main inherited	
						360.8		375.7		0.429		0.058			0.86			
		7.1	197.0	434.3	2.2		3.3		80.1		3.676		0.946	0.257		0.5	main inherited	
						363.5		365.4		0.431		0.058			0.14			
		3.1	477.1	164.7	0.3		3.0		60.6		2.822		0.846	0.300		2.1	main inherited	
						363.9		371.4		0.432		0.058			0.54			
		4.1	530.2	1041.1	2.0		3.0		27.9		1.492		0.829	0.556		2.3	main inherited	
						366.2		374.4		0.436		0.058			0.19			
		1.1	341.3	517.8	1.5		3.8		39.2		2.041		1.060	0.519		3.4	main inherited	
						366.9		379.4		0.438		0.059			0.26			
		6.1	294.2	28.4	0.1		3.2		48.9		2.342		0.893	0.381		−3.1	main inherited	
						368.7		357.8		0.436		0.059			0.26			
		5.1	954.6	6118.5	6.4		2.9		27.4		1.462		0.800	0.547		9.2	main inherited	
						370.4		406.9		0.447		0.059			0.51			
		10.1	218.0	139.4	0.6		3.4		58.6		2.805		0.941	0.335		19.4	inherited	d >|10|%
						374.3		461.4		0.463		0.060			0.72			
		9.1	311.5	518.6	1.7		3.3		46.1		2.228		0.890	0.399		−5.2	inherited	
						377.5		359.3		0.447		0.060			0.18			
		14.1	148.2	242.7	1.6		4.4		156.3		7.044		1.160	0.165		−2.5	inherited	$^{206}Pb_C$ > 1% , σ > 5%
						387.6		378.5		0.463		0.062			1.11			
		13.1	527.0	170.0	0.3		3.3		31.8		1.657		0.867	0.524		−3.3	inherited	
						388.8		376.6		0.464		0.062			0.07			
GS18003	571	3.2	218.3	210.2	1.0		4.3		143.8		6.515		1.273	0.195		8.3	Pb loss	σ > 5%
						344.8		375.3		0.410		0.055			0.79			
		6.1	167.8	85.7	0.5		3.6		166.7		7.464		1.066	0.143		4.2	Pb loss	$^{206}Pb_C$ > 1% , σ > 5%
						345.6		360.3		0.408		0.055			1.21			
		5.2	380.7	147.8	0.4		3.6		82.5		3.808		1.055	0.277		4.2	emplacement	
						349.6		364.4		0.414		0.056			0.68			
		4.1	227.9	100.1	0.4		3.5		123.3		5.536		1.012	0.183		−4.3	emplacement	
						352.9		338.7		0.413		0.056			0.72			
		10.1	457.8	519.5	1.1		3.0		52.7		2.480		0.865	0.349		−7.3	emplacement	
						352.9		329.6		0.411		0.056			0.32			
		2.2	118.6	78.0	0.7		4.1		172.7		7.788		1.193	0.153		9.8	emplacement	$^{206}Pb_C$ > 1% , σ > 5%
						353.5		390.8		0.423		0.056			1.04			
		7.1	176.2	150.3	0.9		3.6		114.7		5.166		1.036	0.201		−6.2	emplacement	
						353.8		333.6		0.413		0.056			0.80			
		3.1	494.7	452.1	0.9		3.0		53.9		2.540		0.863	0.340		0.4	emplacement	

(*continued on next page*)

Table 2 (*continued*)

Drill hole	Depth (m)	Spot n°	U (ppm)	Th (ppm)	Th/U	$^{206}Pb/^{238}U$ (Ma)	1 σ (abs)	$^{207}Pb/^{206}Pb$ (Ma)	1 σ (abs)	$^{207}Pb/^{235}U$	1 σ (%)	$^{206}Pb/^{238}U$	1 σ (%)	error corr.	$^{206}Pb_c$ (%)	disc. (%)	interpreted fraction	notes
						355.1		356.5		0.419		0.057			0.46			
		11.1	173.9	146.4	0.8		3.6		116.1		5.244		1.042	0.199		−0.3	emplacement	
						356.3		355.3		0.420		0.057			0.82			
		5.1	901.2	667.4	0.7		2.8		32.9		1.670		0.812	0.486		1.0	emplacement	
						358.8		362.5		0.424		0.057			0.32			
		1.1	259.6	173.1	0.7		3.3		86.4		3.947		0.954	0.242		0.2	emplacement	
						359.2		359.9		0.425		0.057			0.73			
		2.1	201.9	172.1	0.9		3.6		142.0		6.381		1.035	0.162		0.7	emplacement	σ > 5%
						361.1		363.5		0.427		0.058			0.87			
		12.1	395.1	227.8	0.6		3.1		55.3		2.599		0.878	0.338		−4.5	emplacement	
						362.6		347.5		0.426		0.058			0.40			
		8.2	431.9	248.7	0.6		9.1		188.9		8.734		2.551	0.292		−5.2	emplacement	$^{206}Pb_C$ > 1% , σ > 5%
						366.1		348.5		0.431		0.058			1.59			
		9.1*	997.7	677.3	0.7	**464.7**	9.9		96.4		4.749		2.214	0.466		−77.4	pre-Devonian	d >|10|%
								266.0		0.531		0.075			0.28			
		8.1*	478.1	260.1	0.5	**540.4**	9.9		310.9		13.868		1.918	0.138		−60.7	pre-Devonian	d >|10|%, $^{206}Pb_C$ > 1% , σ > 5%
								341.6		0.643		0.087			17.13			

*: discharged analysis due to its very high reverse discordances or $^{206}Pb_C > 3.5\%$.
ages and isotopic ratios: ^{204}Pb corrected.
Common $^{206}Pb_C$ (%): percentage of non-radiogenic ^{206}Pb according to ^{207}Pb correction method.

was performed in the "non-magnetic" fraction. For further details on the methodology used for the separation procedure, see Lains Amaral et al. (submitted).

At the High-Resolution Geochronology Laboratory (GeoLab-SHRIMP) of the Institute of Geosciences of the University of São Paulo, Brazil zircons were handpicked under a binocular microscope and mounted, together with the standard, in epoxy and polished. Furthermore, detailed imaging was carried out using cathodoluminescence (CL) and backscattered electron (BSE) imaging. The analysed zircons are presented in Figs. A1-A11 (Supplementary data 1; Appendix A).

4.2. U-Pb SHRIMP-IIe zircon analysis

The zircon grains from each sample were mounted in epoxy resin, polished to approximately half of their mean grain thickness for further imaging with transmitted light. After coating with Au, CL images of the zircon grains internal textures were obtained using a Quanta 250 FEG scanning electron microscope equipped with Mono CL3 + CL spectroscope (Centaurus) at the Geochronological Research Centre of the University of São Paulo (CPGeo-USP), Brazil. The conditions used in CL analysis were as follow: 60 μA emission current, 15.0 kV accelerating voltage, 7 μm beam diameter, 200 μs acquisition time, and a resolution of 1024 × 884 pixels.

The U-Pb zircon analyses were carried out with the SHRIMP-IIe at the High-Resolution Geochronology Laboratory (GeoLab-SHRIMP) at the University of São Paulo and the equipment conditions and data acquisition procedures are similar to those described in Williams (1998). Data acquisition was performed with six mass range scans for each of the selected zircon grains with one standard every four zircons. The analysed spots had a size of 24 μm reflecting the diameter of the primary beam and at each analysis the masses of $^{196}(Zr_2O)$, ^{206}Pb, ^{207}Pb, ^{208}Pb, ^{238}U and $^{248}(ThO)$ were measured. Calibration of $^{206}Pb/^{238}U$ age was done using the age of the TEMORA reference zircon which is 417 Ma (Black et al., 2004, 2003). Correction for common Pb was made based on ^{204}Pb measured, and the typical error for the $^{206}Pb/^{238}U$ ratio was <2%; uranium abundance and U/Pb ratios were calibrated against the TEMORA-2 reference material. The technical parameters of SHRIMP-IIe of the GeoLab-SHRIMP, as well as the analytical procedures used, are described in detail in Sato et al. (2014).

In order to calculate the ages, adjustments for common Pb were made with the measured ^{204}Pb and the relevant common Pb compositions from the Stacey and Kramers (1975) proposed model. For data evaluation and reduction SQUID-1.06 software (Ludwig, 2009) was used and for age calculation was used Isoplot® version 4.15 software application (Ludwig, 2012). Errors are reported as 1σ and ages have been calculated at the 95% confidence level (Table 2).

Age plots and corresponding age calculations were performed using the Microsoft Excel add-in Isoplot® (Ludwig, 2012), downloaded from the Berkeley Geochronology Centre website. All calculated age errors in the main text, in Table 3, in Figs. 5–7 and in the Supplementary data are presented as 2σ. In Figs. 5–7, error ellipses are at 2σ. In Figs. B1 to L11 (Supplementary data 2; Appendix A), error ellipses and weighted-average error bars are represented as 1σ.

5. U-Pb SHRIMP results

5.1. Zircon morphology

Under a binocular microscope, the Aljustrel zircons are transparent with visible fractures and occasional inclusions (dark circles and blebs). Prismatic zircons, doubly terminated (e.g. #12 PM15001-521.3; Fig. A8 in Appendix A), were frequently retrieved, with small pyramidal terminations (e.g. #11 ES16005-620.2; Fig. A3). Equant zircons are rarely visible. Subhedral to rounded zircons were also recovered (e.g. #2 GS18003-571; Fig. A11). Sample PM15001-521.3 of the Megacrystal Volcanic Unit provided significantly more zircons than Mine Volcanic

Table 3
Summary table with sample location, lithology, geochemical classification and calculated ages (all errors are reported at 2σ).

Deposit	Drill hole	Depth (m)	Location	Chemo type	Lithology	Pb loss age in Ma (n)	Emplacement age in Ma (n)	Devonian inherited age in Ma (n)	Pre-Devonian inherited age in Ma(n)	Total spots (n)
Feitais	**FS19001**	**182.5**	~5 m below MS; moderate py diss	RHY A	phyric massive rhyolite (coherent)	343.3 ± 3.8 (4)	354.6 ± 2.3 (9)	366.0 ± 6.8 (1) 373.4 ± 7.2 (1)		15
	FS17004	**327.8**	~50 m below MS; residual py diss	RHY A	phyric massive rhyolite (coherent)		356.5 ± 2.6 (6)	365.7 ± 4.3 (2) 373.4 ± 5.8 (1) 406.1 ± 9.0 (1)	492.1 ± 10.2 (1)	11
Estação	**ES16005**	**620.2**	within Jaspers	RHY C	crystal-rich, magnetite-rich, strongly altered massive rhyolite		357.1 ± 2.7 (7)	364.7 ± 2.7 (6) 370.1 ± 4.2 (3) 380.2 ± 6.6 (1)	531.2 ± 10.4 (1)	18
	ES16005	**635**	10 m below Jaspers and 10 m above MS	RHY C	crystal-rich massive rhyodacite (autoclastic?)	332.4 ± 5.1 (2)	354.9 ± 1.9 (11)	373.4 ± 3.4 (4)		17
Algares	**AS18007**	**436**	~60 m below incpient STWK zone	RHY B	aphyric massive rhyodacite (autoclastic?)	324.2 ± 7.0 (1)	353.3 ± 2.4 (8)	367.3 ± 4.1 (3) 376.4 ± 6.6 (1) 403.8 ± 10.8 (1)	421.1 ± 7.6 (1) 518.8 ± 8.0 (1) 537.9 ± 8.4 (1)	17
	AS18005	**359.5**	~6 m below MS; residual py diss	RHY B	phyric massive rhyodacite (coherent)	342.7 ± 5.6 (4)	358.2 ± 2.8	369.2 ± 2.7 (7) 383.4 ± 7.4 (1)		17
	AS18003	**359.3**	incipient STWK zone; drill hole without MS	RHY B	blackish massive rhyodacite (chloritite)	279.5 ± 6.0 (1) 323.1 ± 7.2 (1) 338.4 ± 6.4 (1)	356.3 ± 2.8 (5) or 350.7 ± 4.9 (2) 359.0 ± 3.4 (3)	362.5 ± 4.3 (2) 370.9 ± 5.9 (2) 382.4 ± 6.4 (1) 405.1 ± 43.6 (1)		14
Step-out	**PM15001**	**521.3**	reverse limb; incipient py diss	RHY M	phyric, with megacrysts, massive dacite (autoclastic?)	340.0 ± 7.1 (2)	354.7 ± 2.5 (8)	366.5 ± 8.2 (1) 380.6 ± 4.7 (2)		14
Moinho	**MM16015**	**168**	5 m below MS (fault contact); moderate STWK zone	RHY B	massive rhyolite (autoclastic?)		358.9 ± 2.0 (12)	369.9 ± 5.5 (2) 382.3 ± 7.0 (1) 390.2 ± 8.4 (1)		16
São João	**JS15001**	**407**	5 m below MS after fault	RHY Z	greenish massive rhyodacite (sericitic)			364.4 ± 2.1 (10) 376.0 ± 4.7 (2) 388.3 ± 5.2 (2)		14
Gavião	**GS18003**	**571**	intense STWK zone; ~14 m above MS	RHY B	blackish massive rhyodacite (chloritite)	345.2 ± 5.5 (2)	356.3 ± 2.0 (12)		464.7 ± 19.8 (1) 540.4 ± 19.8 (1)	16

age: discharged single ages due to very high reverse discordance.
age: Concordia or single ages of which all or the majority of single analysis do have d < |10|%, $^{206}Pb_C$ < 1% , σ < 5%.
MS: Massive sulphides; STWK: stinger sulphides; py diss: pyrite disseminations.

Unit samples. In addition, larger and elongated zircons (e.g. #1 PM15001-521.3; Fig. A8) were common in the megacrystal volcanic rock sample, while in the Mine Volcanic rocks the retrieved zircons were stubby to slightly elongated zircons. Long axes are mostly comprised between 80 and 150 μm with an overall range of 40–350 μm, whereas the short axes were 40 to 100 μm.

Back-scattered electron microscopy images (Fig. A1-A11) shows common presence of inclusions (e.g. #2 AS18007-436; Fig. A5) and of inner and transverse fractures, with low or, more frequently, high reflectivity (e.g. #18.1b ES16005-635; Fig. A4). CL images (Figs. A1-A11) frequently show fine oscillatory zoning (e.g. #2 AS18007-436; Fig. A5) and complex zoning (unzoned rims or cores; different zoning patterns in the core and in the rim). More rarely, it was also identified: thick oscillatory zoning (e.g. #6.1 AS18005-359.5; Fig. A6), ghost zoning (#7 FS17004-327.8 and #2 JS15001-407; Fig. A2 and Fig. A10), convoluted primary (?) zoning (#5.1 ES16005-620; #23 ES16005-635 and #7 AS18003-359.3; Fig. A3, A4 and A7); blurred zones (#13 AS18003-359.3; #10 and #2 MM16005-168; Fig. A7 and A9); sector zoning (#8.1 AS18003-359.3 and #12 GS18003-571; Figs. A7 and A11); local reabsorption textures (?) (#7 FS17004-327.8; #5 and #8 GS18003-571; Fig. A2 and A11); embayment textures (?) (#3, #4 and #12 AS18005-359.5; Fig. A6); metamictic dark cores, occasionally associated with radial fractures (#3, #6, #10 FS19001-182.5; #5 PM15001-521.3; #5.1 JS15001-407; Figs. A1, A8 and A10); and unzoned homogeneous metamictic (?) grey to dark zones (#2, #3 FS17004-327.8; #2 GS18003-571; Figs. A2 and A11).

5.2. SHRIMP U-Pb ages of the volcanic rocks of Aljustrel

The individual analytical results of U-Pb isotopes corrected to ^{204}Pb of the 11 representative samples are presented in Table 2 and plotted in Figs. 5–7 and Figs. B1 to L11 (Supplementary data 2; Appendix A). The calculated ages of the 11 samples are summarized in Table 3.

The Aljustrel samples are characterized by variable values of $^{207}Pb/^{206}Pb$ and $^{206}Pb/^{238}U$, suggesting different age populations (Carboniferous, Devonian and Pre-Devonian), as previously proposed by Barrie et al. (2002) and Rosa et al. (2009). An important constraint to determine the ages of the Aljustrel volcanic rocks is given by the palynostratigraphic age (biozone CM) of the metasedimentary sequence (dark shales) that overlies the Aljustrel's volcanic sequence: the Paraíso

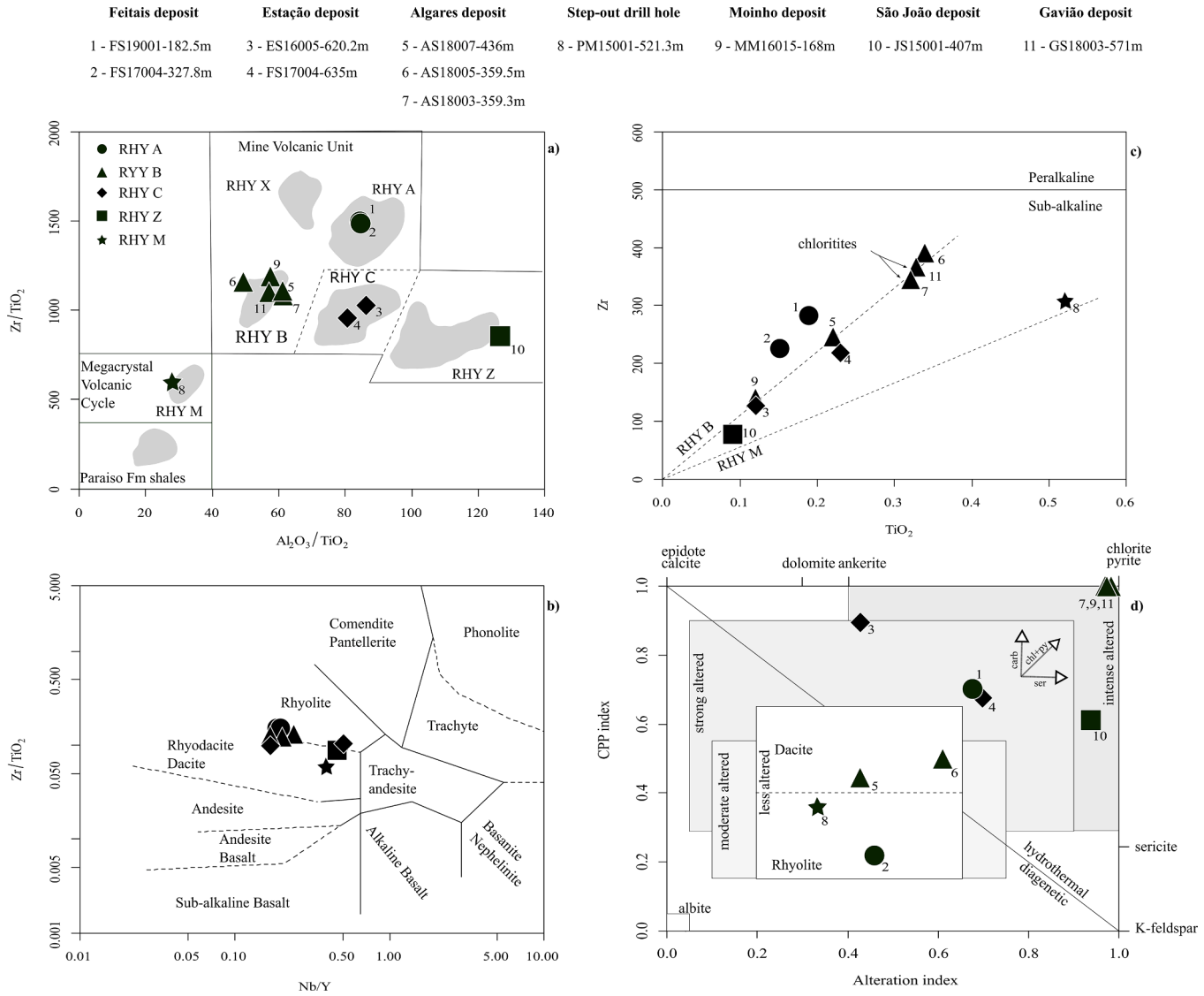

Fig. 3. Immobile element and alteration plots of the 11 geochronological samples selected in this study a) Al_2O_3/TiO_2 vs. Zr/TiO_2, chemostratigraphic type fields (grey areas) after Barrett et al. (2008) and Barrett (2008), main volcanic units and sediments of the Paraíso Fm are schematic and highlighted by straight closed fields; b) Nb/Y vs. Zr/Ti, rock classification diagram (Winchester and Floyd, 1977) c) TiO_2 vs. Zr dashed lines, after Barrett et al. (2008), represent alteration trends resulting from gain or loss in Zr and Ti of the near-constant proportion ($Zr:TiO_2$) chemostratigraphic types RHY B and RHY M. Peralkaline and sub-alkaline felsic fields after Leat et al. (1986); d) Alteration index vs. CPP index, alteration diagram (Large et al., 2001). Alteration boxes adapted from Gifkins et al. (2005) and Large et al. (2001). Arrows represent the apparent main alteration trends of the studied rocks.

Formation and the Gavião Formation. This implies a conservative minimum age near the Visean-Tournaisian boundary – 346.7 ± 0.4 Ma (Cohen et al., 2013) for those formations (Matos et al., 2010; Oliveira et al., 2009). Therefore, zircon grains retrieved in the studied volcanic rocks with $^{206}Pb/^{238}U$ ages younger than 347 Ma, can, with a high degree of confidence, be attributed to Pb loss or resetting.

To evaluate the meaning and accuracy of the obtained Concordia age (preferred age calculation method in this work), we compared it to the weighted average age (using the same zircons of the Concordia age), to the probability density peak age, to the Tuff Zirc age that automatically calculates the youngest coherent group age and to the Unmix age function that automatically calculates the different age populations for a number of populations defined by the user (Ludwig, 2012). In this latter case, to obtain satisfactory results we had to use only post-Silurian zircons and remove the Pb loss fractions. The degree of coherence of the different calculation methods determines the degree of confidence in the obtained results. MSWD values between 1.6 X^2_{red} and 0.4 X^2_{red}, both in the Corcordia and weighted average calculations, were used to validate age populations within the same sample (see further details in Section 6.2).

Pb loss was identified by the behaviour of the youngest fractions of the analyses, such as the presence of a "negative skewed tail" in the probability density plot or a drop tail age in the weighted average plot (as suggested by Spencer et al., 2016). In addition, zircon grains that were identified to have experienced Pb loss using the above method usually show common lead values of $^{206}Pb_c > 1\%$; isotopic ratios percentage errors $^{207}Pb/^{235}U\ \sigma > 5\%$ and/or discordance $<-10\%$ or $>+10\%$) (see Table 2). Zircon grains with at least one of these three characteristics were labelled with a blue colour in the Concordia diagrams and weighted average diagrams in the supplementary figures (Figures B to L; Appendix A).

Hand specimen description for each sample, coupled with immobile elements classifications, is described at the beginning of each section below, taking also into consideration detailed descriptions of previous works (Barriga and Fyfe, 1997; Leitão, 2009). Alteration of the volcanic rocks, such as "chloritization, silicification, sericitization,

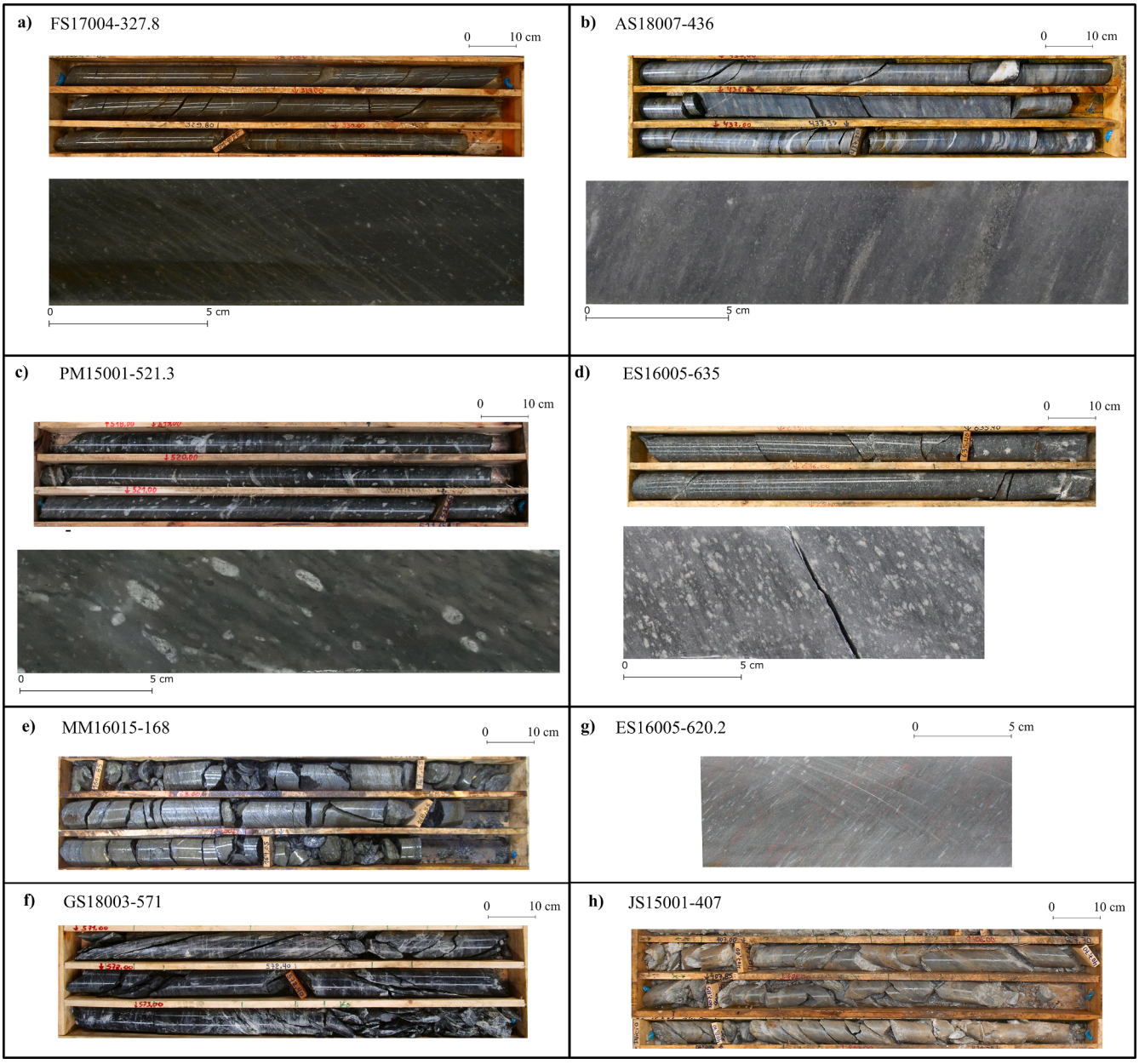

Fig. 4. Chemostratigraphy and volcanic facies of selected geochronological samples: a) FS17004-327.8: feldspar phyric coherent massive rhyolite; RHY A; b) AS18007-436: aphyric autoclastic (?) massive rhyodacite; RHY B; c) ES16005-635: crystal-rich autoclastic (?) rhyodacite; RHY C; d) phyric, with megacrystal, autolcastic (?) massive rhyodacite; RHY M. e) MM16015-168: *feldspar phyric massive rhyodacite; RHY B*; f) GS18003-407: chloritized rhyodacite, RHY B; g) ES16005-620.2: crystal-rich, magnetite-rich, jasper lithic(?)-rich, massive granule to mudstone, strongly altered rock, unknown facies; h) JS15001-407: sericitized rhyodacite; RHY B.

carbonatization, and sulphydization" (Barrett et al., 2008), has been previously identified in detail by other authors. Barriga and Fyfe (1997) also refer that partial to complete sericitization of the feldspar phenocrysts is a common feature in the Aljustrel volcanic rocks associated with the ore mineralization. In this work, alteration description also took into account Gifkins et al. (2005) nomenclature and alteration box-plot of Fig. 3d.

5.2.1. Feitais deposit (drill hole FS19001-182.5m)

This sample was taken 5 m below a massive sulphide lens (Fig. 2a) and it is composed of moderately to highly phyric, with fine-grained feldspar crystals, massive rhyolite (Fig. 3b; RHY A chemotype in Fig. 3a). The alteration is moderately pervasive chloritic, weakly pervasive sericitic and moderately disseminated pyritic. In Fig. 3d, this sample plots within the strong alteration box. Foliation is highlighted by variations in chlorite, sericite and pyrite content. Some phenocrysts are parallel to the foliation, deformed and stretched.

Fifteen zircon spots were analysed, of which 4 were interpreted to have experienced Pb loss, showing errors $^{207}Pb/^{235}U$ $\sigma > 5\%$ and high common lead $^{206}Pb_c > 1\%$. The youngest one is also highly discordant (32.1%). These four grains yield a Concordia age of 343.3 ± 3.8 Ma and a weighted average of 343.3 ± 3.7 Ma (Figs. B3-B4).

Nine concordant zircon spot analyses, of which two present errors $^{207}Pb/^{235}U$ $\sigma > 5\%$, $^{206}Pb_c > 1\%$ or discordance $> |10\%|$, yield a concordant and a weighted average age of **354.6 ± 2.3** Ma and 354.6 ± 2.2 Ma, respectively (Fig. 5a; Figs. B5-B6; Table 3). These results, interpreted as the emplacement age, are in agreement with the youngest Unmix age (354.6 ± 2.6 Ma; Fig. B7). Tuff Zirc algorithm excluded from

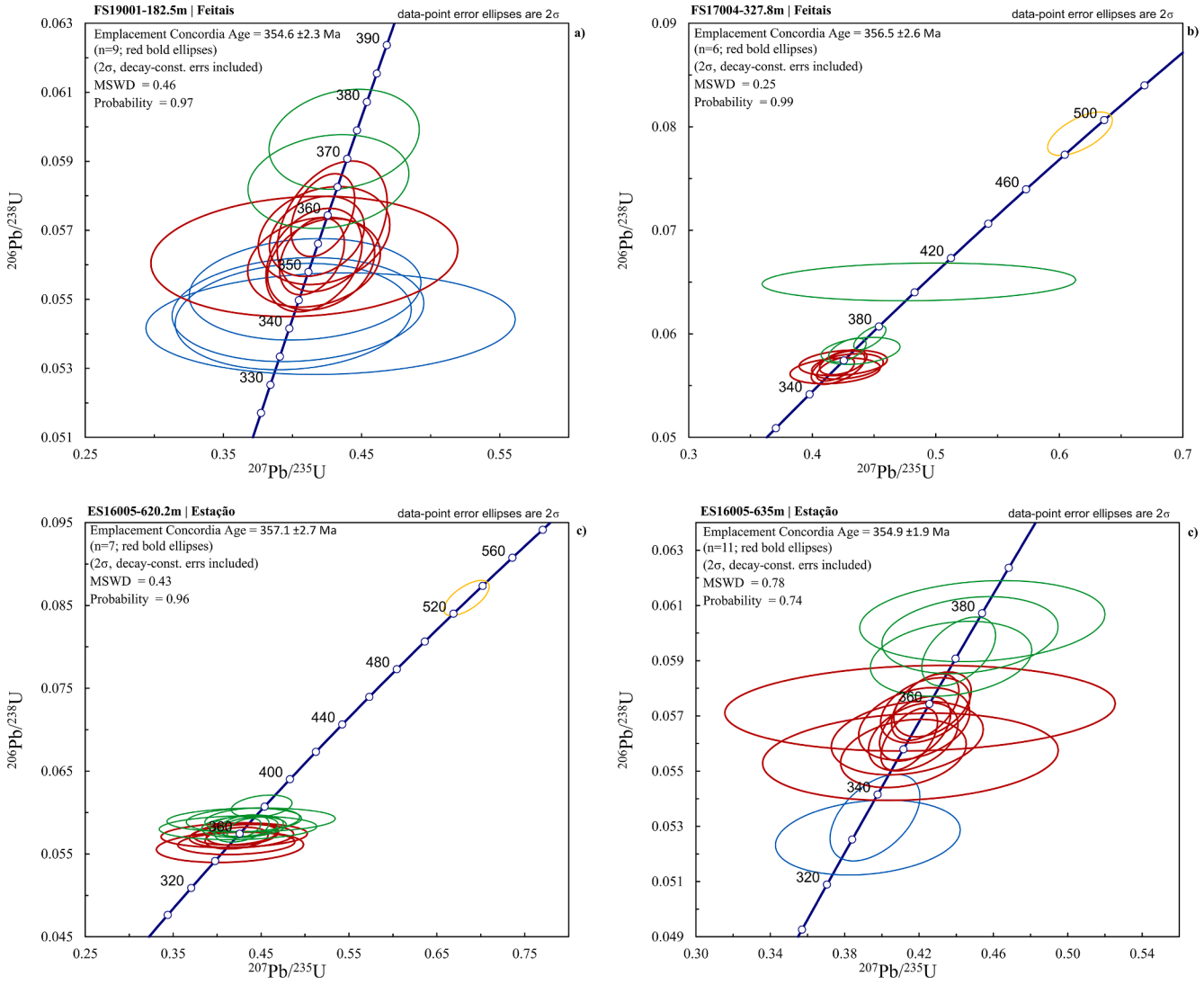

Fig. 5. Concordia diagrams of zircon U-Pb SHRIMP results for Feitais and Estação samples: a) FS19001-182.5; b) FS17004-327.8; c) ES16005-620.2 and d) ES16005-635. Error ellipses are represented as 2σ. Concordia age is of the emplacement analyses (bold ellipses). MSWD and probability values are for combined concordance and equivalence. Blue ellipses: Pb loss analyses; red ellipses: emplacement analyses; green ellipses: inherited Devonian analyses; yellow ellipses: pre-Devonian inherited analyses (online version).

its calculation 2 of the 4 grains with Pb loss, resulting in a slightly younger age (352.7 + 3.7–1.8 Ma; Fig. B7). Probability density peak age is ~353 Ma (Fig. B8).

One grain (#11; Fig. A1), presenting concentric oscillatory zoning, was analysed in the rim and core, providing approximately identical individual $^{206}Pb/^{238}U$ ages of ~352 Ma. Grain #6 (Fig. A1) provided an age of 356.3 ± 5.8 Ma in its core, which was considered as the emplacement age, and in its rim as a Pb loss age (~342 Ma). This grain has a dark core and a lighter rim.

Two single spots provided older $^{206}Pb/^{238}U$ ages of ~366 Ma and ~373 Ma.

Th/U ratios are, compared to other samples, more homogeneous, with an average of 0.53 ± 0.08, varying between 0.42 and 0.67 (Table 2). Th/U ratio decreases from core to the rim with a ratio of 0.6 at the core and 0.4 at the rim in grain #6, whereas in grain #11 it decreases from 0.7 to 0.6.

5.2.2. Feitais deposit (drill hole FS17004-327.8m)

Zircons were retrieved from a sample taken in a weakly mineralized zone, 50 m below the massive sulphide lens. This sample (Fig. 4a) is moderately phyric, fine to medium grain feldspar-rich, massive rhyolite (Fig. 3b), plotting in the RHY A field (Fig. 3a). Alteration is weakly pervasive sericitic and siliceous and weakly disseminated pyritic with some carbonate veinlets.

Eleven isotopic analyses were undertaken. A concordant age of **356.5 ± 2.6** Ma and a weighted average age of 356.4 ± 2.5 Ma, which are identical to Tuff Zirc age (356.5 + 9.2–2.6 Ma), youngest Unmix age (356.5 ± 2.7) and probability density peak age (~356 Ma), were obtained with 6 zircons, of which one has a discordance of 10.5% (Table 2; Table 3; Fig. 5b; Figs. C5, C6, C9 and C10). These highly consistent ages are interpreted as the emplacement age of the rock.

Devonian inherited fractions were identified: 2 grains have a concordant age of 365.7 ± 4.3 Ma (Fig. C7), a single grain present a $^{206}Pb/^{238}U$ age of 373.4 ± 5.8 Ma and another grain (with $^{206}Pb_c > 1\%$ and $^{207}Pb/^{235}U$ σ > 5%) shows a $^{206}Pb/^{238}U$ age of 406.1 ± 9.0 Ma (Table 2; Fig. C11).

A pre-Devonian zircon with a single spot $^{206}Pb/^{238}U$ age of 492.1 ± 10.2 Ma was also identified (Table 2; Fig. C11).

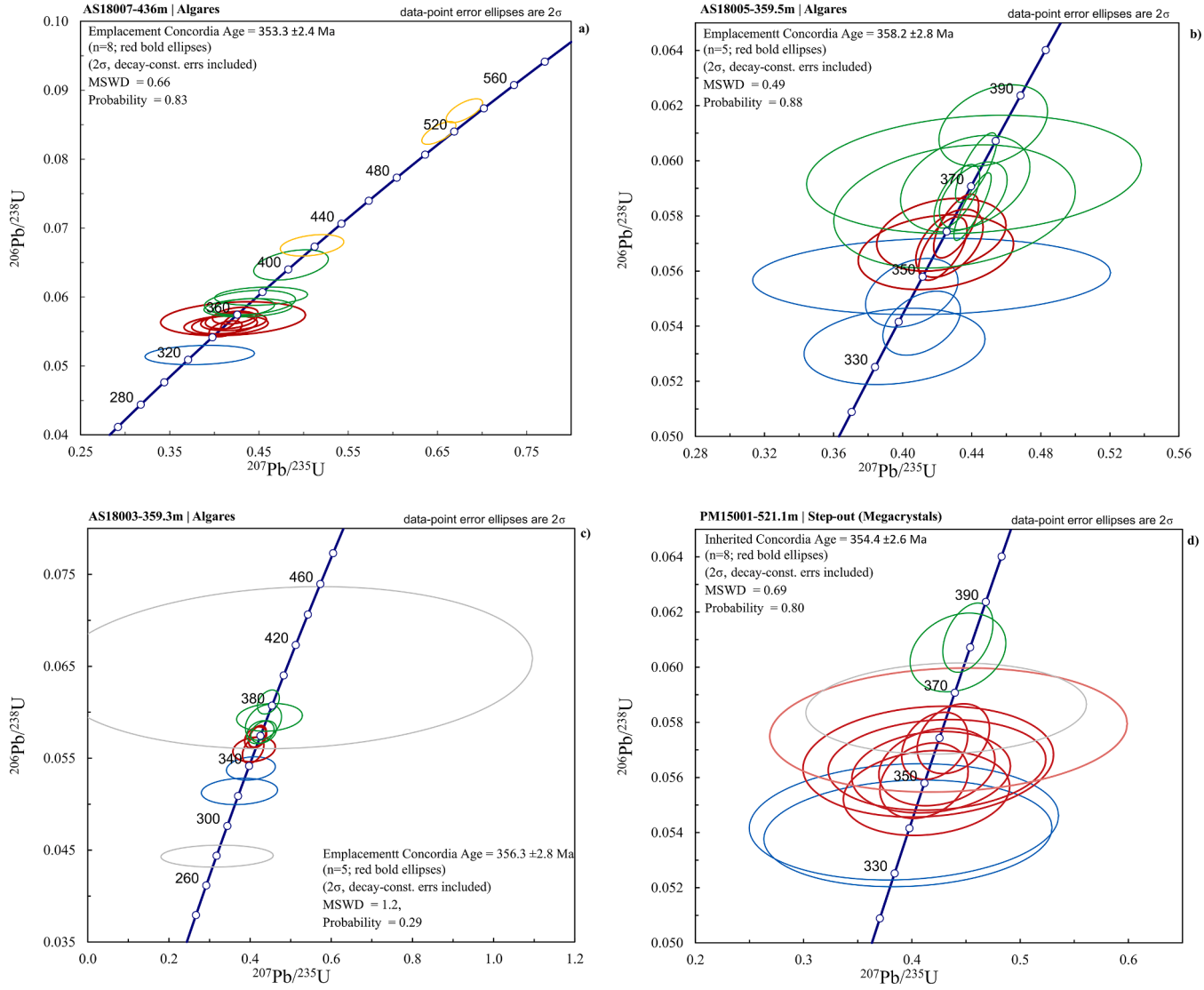

Fig. 6. Concordia diagrams of zircon U-Pb SHRIMP results for Algares and step-out samples: a) AS18007-436; b) AS18005-359.5; c) AS18003-359.3 and d) PM15001-521.3. Error ellipses are represented as 2σ. Concordia age is of the emplacement analyses (bold ellipses). MSWD and probability values are for combined concordance and equivalence. Blue ellipses: Pb loss analyses; red ellipses: emplacement analyses; green ellipses: inherited Devonian analyses; yellow ellipses: pre-Devonian inherited analyses; grey ellipses: excluded analyses (online version).

The average Th/U ratio of the emplacement fraction is 0.76 ± 0.16, varying between 0.92 and 0.54 and of the inherited fractions is 0.48 ± 0.06, ranging from 0.56 to 0.39. The Cambrian zircon has a Th/U ratio of 0.36 (Table 2).

5.2.3. *Estação deposit (drill hole ES16005-620.2m)*

Zircons were extracted from a massive level of strongly foliated rhyolite (chemotype RHY C; Fig. 3a-b) within a chert level (Fig. 2b). The rock is moderately pervasive chloritic and sericitic, magnetite-rich, clast supported, lithic-rich (?) (reddish jasper, volcanic and crystal-rich) massive granule to mudstone (Fig. 4g). Jasper occurs in millimetric patchy layers resembling alteration. There are frequent whitish fine-grain fragments, occasionally presenting sigmoid features (probably carbonates; see also Fig. 3d). Due to strong hydrothermal alteration and deformation, it is not possible to be completely sure of the volcanic facies of this sample.

Eighteen zircons were analysed. Emplacement concordant age of **357.1 ± 2.7 Ma** was obtained using the youngest grain cluster composed of 7 zircons (4 grains have high $^{206}Pb_c > 1\%$ and $^{207}Pb/^{235}U\ \sigma > 5\%$; Table 2), which is coincident with the obtained weighted average age and similar to the youngest Unmix age (357.2 ± 3.6 Ma) (Fig. 5c; Figs. D5, D6 and D11; Table 3). Although statistically accurate regarding MSWD and probability values, we can observe in the emplacement weighted average diagram that the distribution of the emplacement grains is not homogenous (Fig. D6), with the 2 youngest grains presenting a biased Pb loss alike pattern (both with $^{206}Pb_c > 1\%$ and $^{207}Pb/^{235}U\ \sigma > 5\%$).

The Concordia age and weighted average age obtained for the inherited fraction was 364.7 ± 2.6 Ma (Figs. D7-8) using 6 zircon grains, of which 2 show $^{206}Pb_c > 1\%$ (of these, one grain has a discordance of ~13%, and $^{207}Pb/^{235}U\ \sigma > 5\%$ as well; Table 2). Probability density peak (~363 Ma) and Tuff Zirc (364.2 + 1.7–4.8 Ma) ages resulted in ages similar to the calculated inherited age; this is due to the fact that an almost identical number of analyses were obtained to calculate the emplacement age (7 grains) and the inherited age (6 grains).

Other two older Devonian fractions were identified, one with a Concordia age of 370.1 ± 4.2 Ma and a weighted average of 370.2 ± 4.2 Ma (3 grains with identical single spot $^{206}Pb/^{238}U$ ages presenting $^{206}Pb_c > 1\%$, $^{207}Pb/^{235}U\ \sigma > 5\%$ or discordance $>|10\%|$, Table 2) and another with a single spot $^{206}Pb/^{238}U$ age of ~380 Ma (Figs. D9, D10

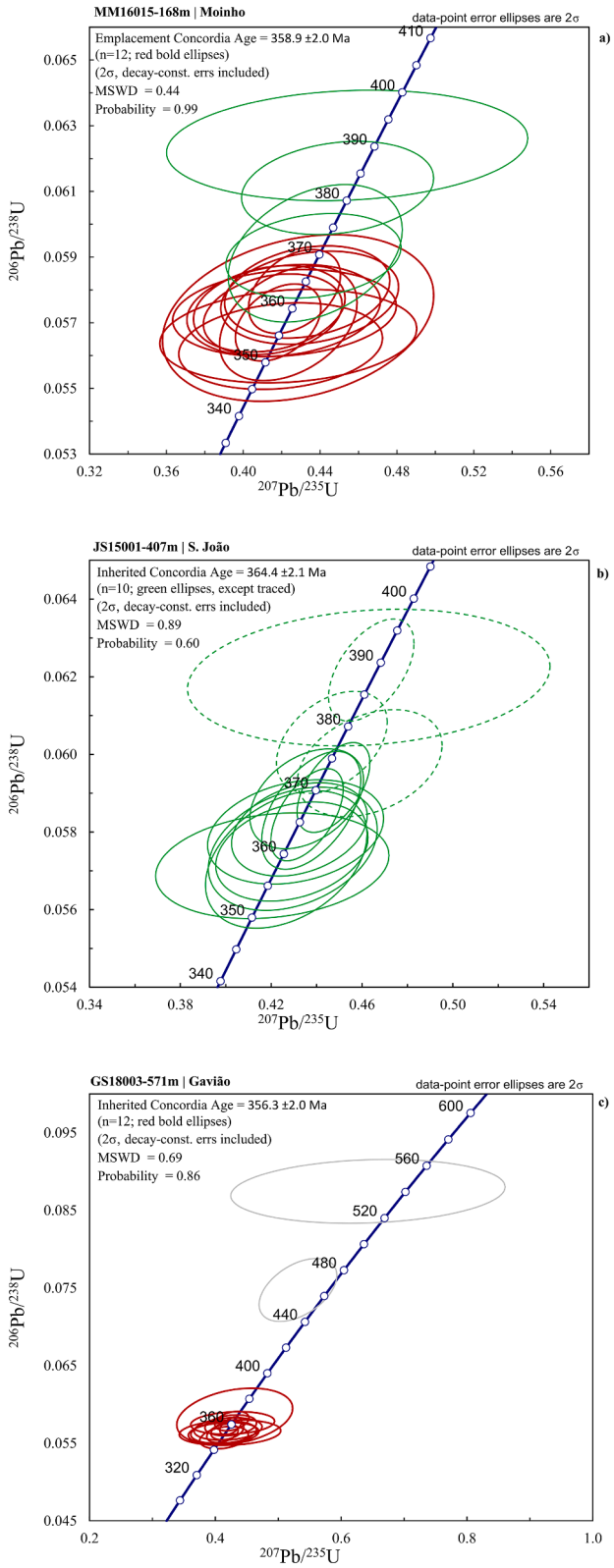

Fig. 7. Concordia diagrams of zircon U-Pb SHRIMP results for Moinho, São João and Gavião samples: a) MM16015-168; b) JS15001-407 and c) GS18003-571. Error ellipses are represented as 2σ. Concordia age is of the emplacement analyses (bold ellipses). In sample JS15001-407, Concordia age is of the inherited analyses (continuous ellipses; see text). MSWD and probability values are for combined concordance and equivalence. Blue ellipses: Pb loss analyses; red ellipses: emplacement analyses; green ellipses: inherited Devonian analyses; grey ellipses: excluded analyses (online version).

and D11)

A pre-Devonian single spot $^{206}Pb/^{238}U$ age of 531.2 ± 10.4 Ma was also retrieved (Fig. D12; Table 2).

The average Th/U ratio of the emplacement fraction is 0.73 ± 0.39, varying between 1.17 and 0.03. The average Th/U ratio of the main inherited fraction is 0.66 ± 0.27, ranging from 1.03 to 0.29 and of the secondary inherited fractions is 0.42 ± 0.08, between 0.32 and 0.53. Zircons with low Th/U ratios (<0.35) all have low Th (<100 ppm), with the exception of the Cambrian grain, which has Th/U ratio of 0.29 and 135 ppm of Th (Table 2).

5.2.4. *Estação deposit (drill hole ES16005-635m)*

This sample was taken ~10 m above the massive sulphides and 10 m below a prominent jasper level (Fig. 2b). The sample is a highly phyric, with medium-grained feldspar crystals, massive rhyodacite (Fig. 4d; Fig. 3b). Fig. 3a indicates a RHY C chemotype signature. Alteration is moderately pervasive sericitic and weakly patchy-banded chloritic. In Fig. 3d, the sample plots within the strong alteration box. Overall, this crystal-rich volcanic rock is foliated. Foliation is given by chloritic alteration and orientation of feldspar crystals, which are generally irregular, locally sigmoidal. The more elongated ones have rounded rims.

Seventeen zircon grains were selected for analysis, of which 2 were interpreted to have experienced Pb loss, one of these (#21.1) did not present any abnormal value, such as $^{206}Pb_c$ > 1%, $^{207}Pb/^{235}U$ σ > 5% and/or discordance >|10%| (Table 2; Fig. D17). These 2 grains yield a Concordia age of 332.4 ± 5.1 Ma.

Emplacement age was obtained with 11 grains, of which only 2 show $^{206}Pb_c$ > 1%, $^{207}Pb/^{235}U$ σ > 5%, that gave a Concordia age and a weighted average age of **354.9 ± 1.9 Ma** (Fig. 5d; Figs. D5-D6; Table 3). Unmix age (354.9 ± 1.9 Ma), Tuff Zirc age (354.5 + 4.5–2.3 Ma) and probability density peak age (~353 Ma) are also in agreement, suggesting that the emplacement age obtained is of great confidence and well represented in the analysed spots (Fig. D9-D10).

It is interesting to note that the box chart presents an artificial (?) stair step pattern at roughly 348 Ma, 353 Ma and 359 Ma (Fig. D2 and D6). This is also observed in other samples (e.g. FS19001-182.5; GS18003-571). The spread of single ages and emplacement ages between ~353 and ~359 Ma will be discussed ahead.

Four grains, of which one has $^{206}Pb_c$ > 1% and $^{207}Pb/^{235}U$ σ > 5%, gave an inherited concordant age of 373.4 ± 3.4 Ma, which is in agreement with weighted average age (373.5 ± 3.4 Ma) and with inherited Unmix age (372.1 ± 3.8 Ma) (Fig. D7-D9).

The average Th/U ratio of the emplacement fraction is 0.74 ± 0.39, varying between 1.29 and 0.24. The average Th/U ratio of the main inherited fraction is 0.36 ± 0.03, ranging from 0.41 to 0.33. Zircons with low Th/U ratios (<0.35) also have low Th (<100 ppm) (Table 2).

5.2.5. *Algares deposit (drill hole AS18007-436 m)*

This sample was collected 60 m below the mineralized zone and 8 m below a metric blackish shale level (Fig. 2c; Fig. 4b). Zircons were separated from an aphyric massive rhyodacite (Fig. 3b) with weakly spotty carbonate alteration. Weakly selective sericitic and chloritic alteration resembling diffuse clast-like textures that could represent in situ, autoclastic, volcaniclastic features (Fig. 4b). Overall, this sample is weakly altered (Fig. 3d). In Fig. 3a and c, the sample plots in the RHY B chemotype field.

Seventeen zircon grains were analysed, of which the youngest age result is attributed to Pb loss. One grain (#4; Fig. A5), in its core, has an age of ~356 Ma, which was used to obtain the emplacement age (see below) and in its rim, provided an age ~of 371 Ma, which was used to obtain an inherited age (see below). This grain has different growth patterns at the core and at the rim.

A Concordia age of **353.3 ± 2.4 Ma**, based on 8 grains of which 1 grain has $^{207}Pb/^{235}U$ σ > 5%, is interpreted as the emplacement age (Fig. 6a; Table 3). This is further supported by the consistency of the

results with the weighted average age, youngest Unmix age, Tuff Zirc age and youngest probability density peak age (353.2 ± 2.3 Ma, 353.1 ± 2.5 Ma, 353.9 + 2.6 –3.2 Ma and ~353, respectively) (Figs. F4 and F7). This suggests that the emplacement age obtained for this sample was based on statistically consistent and well-represented spot analyses.

A similar age consistency was obtained for the inherited age, although only represented by 3 grains. Concordia age, weighted average age, Unmix age, and probability density peak age gave identical ages (**367.3 ± 4.1 Ma**; 367.3 ± 4.1 Ma; 366.7 ± 5.6 Ma and ~366 Ma, respectively; Fig. F5-F7). In addition, two older Devonian fractions with single spot $^{206}Pb/^{238}U$ ages of 376.3 ± 6.6 Ma (with $^{206}Pb_c > 1\%$) and of 403.8 ± 10.8 Ma were identified, as well as pre-Devonian fractions with single spot $^{206}Pb/^{238}U$ ages of 421.0 ± 7.6 Ma, 518.8 ± 8.0 Ma and 537.9 ± 8.4 Ma. The 2 Cambrian grains show + 11 to + 12% discordance (Fig. E8).

The average Th/U ratio of the post-Silurian zircons is 0.85 ± 0.37, with the larger amplitudes observed in the emplacement fraction, between 1.73 and 0.45. Cambrian zircons have low Th/U ratios, between 0.1 and 0.2 (Table 2). The core of grain #4, with an age of ~356 Ma, provided a Th/U ratio of 0.6, whereas its rim, with an age of ~371 Ma, has a slightly higher Th/U ratio of 0.7.

5.2.6. Algares deposit (drill hole AS18005-359.5 m)

At 359.5 m in drill hole AS18005, zircons were retrieved from a weakly phyric, with fine-grained feldspar crystals, massive rhyodacite (Fig. 3b). Alteration is weakly pervasive sericitic and chloritic and weakly spotty carbonate (Fig. 3d). Foliation is weak to moderate. The sample has a RHY B signature (Fig. 3a, c) and was collected ~6 m below a massive sulphide lens of the Algares deposit (Fig. 2d).

Seventeen spots were analysed. One grain (#8; Fig. A6), in its core, has a Pb loss age (~347 Ma) with no significant common lead, discordance or $^{207}Pb/^{235}U$ σ errors, and in its rim, provided an age of ~359 Ma. This spot was used to obtain the emplacement age (see below). Another grain (#13: Fig. A6) shows the reverse with a youngest Pb loss age at the rim presenting $^{206}Pb_c > 1\%$, probably related to a fracture. Both grains are characterized by cores darker than rims.

The 4 youngest ages are interpreted to have resulted from Pb loss and yielded a Concordia age of 342.7 ± 5.6 Ma (Fig. G3).

Five spot analyses, assigned to the emplacement event, provided a Concordia age of **358.2 ± 2.8** Ma and a similar weighted average age of 358.0 ± 2.7 Ma (Fig. 6b; Figs. G5-G6; Table 3). An inherited age was obtained with 7 zircons, of which 2 grains show $^{206}Pb_c > 1\%$ or $^{207}Pb/^{235}U$ σ > 5% (Table 2). Both Concordia and weighted average methods yield identical ages: **369.2 ± 2.7** Ma and 369.0 ± 2.7 Ma, respectively (Fig. G7-G8). Unmix age peaks resulted in similar ages for both zircon sets (358.3 ± 3 Ma, 368.9 ± 2.9 Ma), which are also roughly coincident with probability density peak ages (~357 Ma, ~367 Ma) (Fig. G9-G10). However, the Tuff Zirc algorithm provided an age of 365.5 + 5.1 –6.2 Ma which is probably due to the greater preponderance of the inherited fraction (7 grains) relative to the emplacement fraction (5 grains). The age obtained by this method is, therefore, biased and reflects an artefact due to a statistical misrepresentation of the events affecting this sample (as in Oliveira et al., 2013; Rossignol et al., 2019). A single concordant zircon analysis of an older, but still Devonian age, gave a $^{206}Pb/^{238}U$ age of ~383 Ma (Fig.G10).

The average Th/U ratio is 0.82 ± 0.36, with the larger amplitudes observed either in the main inherited fraction, between 1.78 and 0.44, and in the emplacement fraction, between 1.45 and 0.43 (Table 2). Grain #13 and grain #8 have higher Th/U ratios in the core than the rim, with Th/U values of 1.1–0.6 and 0.8–0.5, respectively.

5.2.7. Algares deposit (drill hole AS18003-359.3m)

This sample is an intensely altered blackish massive rhyodacite (Fig. 3b, d), located in an incipiently mineralized zone composed mostly of pyritic disseminations. This chloritite has a RHY B chemotype signature (Fig. 3a, c).

Fourteen U-Pb analyses were undertaken, of which 9 resulted in $^{206}Pb_c > 1\%$, and/or discordance >|10%| (Table 2). One grain (#1; Fig. A7), in its core, has an age of 382.4 ± 3.2 Ma and in its rim, provided an age of 405.1 ± 43.6 Ma. The latter was excluded due to its very high common lead (Table 2). Another grain (#9) provided an age of ~359 Ma in its core, which was considered an emplacement age (see below), and in its rim a Pb loss age (~279 Ma). Both grains have brighter rims surrounding dark cores.

Three zircon grains were interpreted as representing Pb loss and the youngest age (~279 Ma) was excluded due to high $^{206}Pb_c$ (~6%).

Five zircon grains, of which 3 are discordant (~12–19%; Table 2), gave a Concordia age of **356.3 ± 2.8 Ma** (Fig. 6c; Fig. H3). The weighted average age for these grains is 356.5 ± 2.8 Ma with a MSWD value of 2.1. This MSWD value is higher than the threshold assumed in this work (see Section 6.2), thus alternative Concordia ages of 350.7 ± 4.9 Ma, two grains, and of 359.0 ± 3.4 Ma, three "blue" grains, are presented in Table 3. However, an emplacement Concordia age using only two grains is, in comparison with the other samples, not statistically relevant. The youngest Unmix age, main probability density peak age and Tuff Zirc age provided the following results: 358.4 ± 2.4 Ma, ~359 Ma and 362.4 + 9.8 –3.6 Ma, respectively (Fig. H7-H8). The small number of good zircon analyses and the high degree of variability of ages obtained with different methods significantly decreases our degree of confidence in the ages obtained for this sample. Our best estimate for the ages of this rock is the emplacement Concordia age that used the 5 zircons (**356.3 ± 2.8 Ma**).

Two Devonian inherited Concordia ages were obtained: 362.5 ± 4.3 Ma, using two grains, and 370.9 ± 5.9 Ma, using two grains, of which one has $^{206}Pb_c > 1\%$ and $^{207}Pb/^{235}U$ σ > 5% (Fig. H5-H8). One zircon provided two discordant (~14–19%) spot analyses with older $^{206}Pb/^{238}U$ ages of ~382 Ma at the core of the grain and ~405 Ma at its rim (Fig. A7). As previously mentioned, this result was discharged due to anomalous $^{206}Pb_c$ values (Table 2).

The average Th/U ratio of the emplacement fraction is 0.90 ± 0.36, ranging from 1.5 to 0.4 and of the inherited fractions is 0.72 ± 0.22, ranging from 1.2 to 0.4 (Table 2).

5.2.8. Step-out drill hole (drill hole PM15001-521.3m)

This sample was collected near the bottom of the PM15001 hole, at 521.3 m. It belongs to the Megacrystal Volcanic Unit and is composed of moderately to abundant quartz-feldspar, fine to coarse grain phyric, massive dacite (Fig. 4c; Fig. 3b) with a RHY M chemotype (Fig. 3a, c). Two size populations of phenocrysts are clearly visible: a fine to medium-grained and a coarser (the megacrysts). Alteration is moderately pervasive siliceous, weakly pervasive sericitic and weakly patchy-veinlet chloritic. In Fig. 3d, this sample plots in the less altered box. Foliation is given by the orientation of chloritic patches (autoclastic?) and the K-feldspar megacrysts (see Barriga and Fyfe, 1997).

Fourteen SHRIMP-IIe analyses were undertaken, of which the 2 youngest $^{206}Pb/^{238}U$ results are attributed to Pb loss yielding a Concordia age of 340.0 ± 7.1 Ma (Fig. I3). These spots resulted in $^{206}Pb_c > 1\%$, $^{207}Pb/^{235}U$ σ > 5% and/or discordance >|10%|.

The emplacement age was obtained with 8 zircon grains, of which 5 show $^{206}Pb_c > 1\%$ and $^{207}Pb/^{235}U$ σ > 5% and 1 has high discordance (~16%), providing a Concordia age and weighted average age of **354.7 ± 2.5** Ma (Fig. 6d; Fig. I5-I6; Table 3). Youngest Unmix extracted age resulted in an identical age value (354.7 ± 2.5 Ma). Tuff Zirc algorithm gave a slightly younger age (353.8 ± 6.0 Ma) (Fig. I9). The probability density peak age is at ~353 Ma (Fig. I10). Overall, age results are in agreement with the calculated emplacement Concordia age.

Devonian inherited fractions were identified in two grains, of which one has a discordance of ~15%, providing a Concordia age of 380.6 ± 4.7 Ma and a weighted average age of 380.7 ± 4.6 Ma (Fig. I7-I10). Grain #14.1 was excluded due to its very high common lead (~8%; Table 2).

The average Th/U ratio of the emplacement fraction is 0.57 ± 0.40,

varying between 1.36 and 0.08 and of the inherited fractions is 0.42 ± 0.21, ranging from 0.70 to 0.17 (Table 2).

5.2.9. Moinho deposit (drill hole MM16015-168m)

The sample was taken from a stockwork zone, 5 m below the massive sulphide lens (Fig. 2e). Zircons were extracted from a massive rhyodacite (Fig. 4e; Fig. 3b) that plots in the RHY B chemotype field (Fig. 3a, c). This sample is intensely altered (Fig. 3d). Chloritic and pyritic alteration defines clast-like textures (autoclastic?).

Sixteen zircon grains were analysed, of which 12 define a Concordia age and weighted average age of **358.9 ± 2.0 Ma** (Fig. 7a; Fig. J3-4; Table 3). Of these 12 grains, 2 have $^{206}Pb_c > 1\%$ and $^{207}Pb/^{235}U\ \sigma > 5\%$ and 2 show discordance > |10%|. Probability density peak (~359 Ma), Tuff Zircon (359.4 + 3.7–2.0 Ma) and youngest Unmix (359.1 ± 2.1 Ma) ages are all consistent with the obtained Concordia age (Fig. J7-J8).

Two grains, with identical single spot ages, yield a Concordia age and weighted average ages of 369.9 ± 5.5 Ma (Fig. J5-J6). The obtained ages, interpreted as inherited, are in accordance with the oldest Unmix age (369 ± 7.1 Ma). In addition, two older Devonian fractions are represented by two grains, with discordance >|10%|, providing single spot $^{206}Pb/^{238}U$ ages of ~382 Ma and ~390 Ma.

The average Th/U ratio of the emplacement fraction is 0.76 ± 0.44, varying between 1.56 and 0.39 and of the inherited fractions is 0.63 ± 0.22, ranging from 0.88 to 0.34 (Table 2).

5.2.10. São João deposit (drill hole JS15001-407 m)

Zircons were extracted from a strongly sericitic, pervasively altered (Fig. 3d), massive level of rhyodacite composition (Fig. 4h; Fig. 3b; RHY Z chemotype in Fig. 3a) with minor pyrite and no visible crystal fragments, just below a massive sulphide lens. The contact between the sulphide lens and the volcanic unit where the sample was collected is faulted (Fig. 2f).

Fourteen spots were selected for analysis. Concordia and weighted average ages **of 364.4 ± 2.1** Ma and 364.3 ± 2.1 Ma were obtained with 10 U-Pb isotopic results that are approximately in accordance with the age extracted by the Tuff Zirc approach (363.7 + 5.0 –4.5 Ma), probability density peak (~363 Ma) and the Unmix algorithm (363.2 ± 3.1 Ma) ages (Fig. 7b; Fig. K3, K4, K8 and K9). These Devonian ages were interpreted as representing an inherited event. We suggest that no grains representing the emplacement event were selected for analysis. The absence of emplacement ages has been reported previously in volcanic rocks of the Iberian Pyrite Belt (Oliveira et al., 2013). It should be also noticed the wide age range of single spot analysis (~358 to ~370 Ma), including two analyses that could be considered as emplacement fractions (<360 Ma; Table 2). However, there is no statistical (e.g. concordant and equivalent MSWD = 1.04) or graphical support (continuous age variation) that may support a valid age separation to obtain an emplacement age that is in accordance with the other emplacement ages at Aljustrel district.

Two concordant grains define an inherited fraction at 376.0 ± 4.7 Ma, of which one has a discordance >|10%|, and another two grains yield a concordant age of 388.3 ± 5.2 Ma, of which one has $^{206}Pb_c > 1\%$ and $^{207}Pb/^{235}U\ \sigma > 5\%$.

This sample shows the highest Th/U ratios of the 10 zircons selected for the main Concordia age (Table 3), with an average of 2.56 ± 1.93, ranging from 6.41 to 0.1. Th/U ratios of the older inherited zircons vary between 1.66 and 0.32 (1.07 ± 0.6).

5.2.11. Gavião deposit (drill hole GS18003-571 m)

This sample, intensely altered into a chloritite (Fig. 3d; Fig. 4f), was collected in a stockwork zone (Fig. 2g). It is a blackish massive rhyodacite (Fig. 4f; Fig. 3b), with pyritic disseminations. It has a RHY B chemotype signature (Fig. 3a, c).

Sixteen spots were performed, of which the 2 youngest single spot results, $^{206}Pb_c > 1\%$ and $^{207}Pb/^{235}U\ \sigma > 5\%$, are interpreted to represent Pb loss. These provide a Concordia age of 345.2 ± 5.5 Ma (Fig. L5-L6). The rest of the analyses are interpreted to represent the emplacement event and define a Concordia age of **356.3 ± 2.0** Ma (Fig. 7c; Fig. L7), which is coherent with the weighted average, Tuff Zirc and Probability density peak ages (356.3 ± 2.0 Ma, 355.7 + 5.3–2.8 Ma, ~355 Ma; respectively) (Fig. L8-L11). In grain #3 (Fig. A11) the results suggest that the core has had Pb loss (~345 Ma), while the rim shows a single spot analysis in accordance with the emplacement age (~355 Ma). The rim and core analyses of grain #5 were both used to obtain the emplacement age mentioned above, with the core presenting an older $^{206}Pb/^{238}U$ age (~359 Ma) than the rim (~350 Ma). The single spot age spread of concordant grains will be discussed ahead. Grain #8 provided an age of 366.1 ± 18.2 Ma in its bright rim, which was considered an emplacement age (see also Section 6.2), whereas its dark core provided a Cambrian age. No Devonian inherited fractions were identified.

Two pre-Devonian spots, showing extreme high negative discordances (-61%, −77%), gave single spot $^{206}Pb/^{238}U$ ages of ~465 Ma and of ~542 Ma. Both analyses were excluded.

The average Th/U ratio of the emplacement fraction is 0.72 ± 0.20, ranging from 1.13 to 0.39. The Ordovician spot has a Th/U ratio of 0.68 and the Cambrian spot has a Th/U ratio of 0.54 (Table 2). Grains #2, #3 and #5 have higher Th/U ratios at the core (0.9, 1 and 0.7, respectively) than at the rim (0.7, 0.7 and 0.4, respectively). In grain #8 the Pre-Devonian spot has a Th/U ratio of 0.5 and the post-Silurian spot has a Th/U ratio of 0.6.

6. Discussion

For the first time, all the known six deposits of the Aljustrel district have been targeted for U-Pb zircon dating of the volcanic rocks that host the mineralization. Isotopic analyses using the SHRIMP-IIe technique were performed in 169 spots from 11 samples.

Summarized in Table 3 are the calculated Concordia and single ages of the 11 samples. They show an almost gradual Concordia age variation between the intervals ~353–359 Ma (83 spots) and ~364–383 Ma (47 spots; in particular between 364 and 373 Ma with 36 spots). In addition, the following fractions were identified in 6 spots: ~386–392 Ma and 403–406 Ma. 14 grains with high Th/U gave a Concordia age of 364.9 ± 2.0 Ma (sample JS15001-407). Additionally, 18 single ages were attributed to Pb loss (~324–345 Ma) and 7 spots provided the pre-Devonian ages (Silurian and Cambrian), of which two were attributed to possible Pb gain.

6.1. Pb loss, common lead and discordance

Pb loss, high content of common Pb and high discordance have been previously noticed in the zircons of the volcanic rocks of the IPB (Barrie et al., 2002; Nesbitt et al., 1999; Paslawski et al., 2020; Rosa et al., 2009).

Higher contents of common Pb are often associated with higher analytical errors, which are a direct result of the common Pb correction. This is particularly visible when $^{206}Pb_c$ is >1%. Nonetheless, zircons with $^{206}Pb_c > 1\%$ still give valuable information, namely for less representative inherited fractions (e.g. ~406 Ma in sample FS17004-327.8; Table 3) when balanced with at least one analysis without $^{206}Pb_c > 1\%$, $^{207}Pb/^{235}U\ \sigma > 5\%$ and/or discordance >|10%|. Very high common lead analyses were excluded ($^{206}Pb_c > 3.5\%$; Table 2). Regarding the Concordia diagrams, the effect of inserting analyses with $^{206}Pb_c > 1\%$ in a group of more precise analyses did not affect significantly the Concordia age calculations (e.g. MM16015-168). However, in sample ES16005-620.2, which is strongly altered, if we exclude the 4 spots having $^{206}Pb_c > 1\%$, it would have given an age of 358.8 ± 1.9 Ma (3 grains), while considering the 4 higher common Pb analysis the Concordia age is 357.1 ± 2.7 Ma (7 grains). These ages, however, are identical within error.

In this work, we used “negative skewed tail” in the probability density plot or an age drop tail in the weighted average diagram to

identify grains that have experienced significant Pb loss. This method (Spencer et al., 2016) has proved to be effective in the Aljustrel volcanic rocks and it is consistent with the age constraints given by palynostratigraphic dating of the upper VSC (~347 Ma).

However, when we plot all the spots in the probability density diagram the obtained curve is near-Gaussian (Fig. 8a), which is a direct result of precision errors and the existence of grains with Pb loss, which provided ages that are only 10–25 Ma younger (~330–345 Ma; Fig. 8b) than the emplacement age (353–359 Ma, Fig. 8c). By removing the 18 Pb loss grains, the curve becomes clearly asymmetrical (positive-skewed, not shown), which suggests more than one magmatic event (see Sections 6.2 and 6.4).

In this work, all the error ellipses (1 σ) of the post-Silurian measurements intersect the Concordia, which includes grains with discordances up to 20% (normal discordance) or down to −20% (reverse discordance). According to Ireland and Williams (2003) and Spencer et al. (2016), the steep dip curvature of the Concordia combined with the slightly more imprecise measurement of the ^{207}Pb for ages below 400 Ma implies that relative discordance of Phanerozoic zircons is often within the in-situ U-Pb error measurements. Thus, for igneous rocks younger than 400 Ma which have been analysed with in-situ methods, it may also be relevant to validate or reject the analysis based on its relationship with the Concordia. Nonetheless, in Supplementary data 2 (Appendix A) we have coloured the analyses with relative discordance higher than 10% or lower than −10%, highlighting potential error age calculations. A good example is sample AS18003-359.3 (a chloritite) of which 3 of the 5 analyses obtained for the emplacement age have a discordance above |10|%. Without considering these 3 analyses, the obtained emplacement age (356.3 ± 2.8 Ma) would have been 350.7 ± 4.9 Ma (Table 3, see further discussion in 6.2).

Interestingly, reverse relative discordance (i.e. ^{206}Pb/^{238}U age > ^{207}Pb/^{206}Pb age) is quite common in this work. In fact, 84 of the 169 grains (i.e. 50%) show reverse discordance (−0.2% to −74%). It is also common in previous LA-ICP-MS IPB works (Oliveira et al., 2013; Paslawski et al., 2020; Rosa et al., 2009), in which 143 of the 429 analysis (i.e. 33%) show reverse discordance (−0.3% to −12%). Although slight reverse discordance can be attributed to error measurements, in particular for zircons younger than 400 Ma (see above), it does not explain the extreme high reverse discordance of the two pre-Devonian grains of this work: #9.1 and #8.1 of sample GS18003-571. Grain #9.1 has a single ^{206}Pb/^{238}U age of 464.7 ± 19.8 Ma (−77.4% discordant) and grain #8.1 has a single ^{206}Pb/^{238}U age of 540.4 ± 19.8 Ma (−58.4% discordant).

Previously higher precision measurement results (i.e. ID-TIMS; Barrie et al., 2002; Donaire et al., 2020; Valenzuela et al., 2011) in the volcanic rocks of the IPB show 11 of 85 grains (i.e. ~13%) with reverse

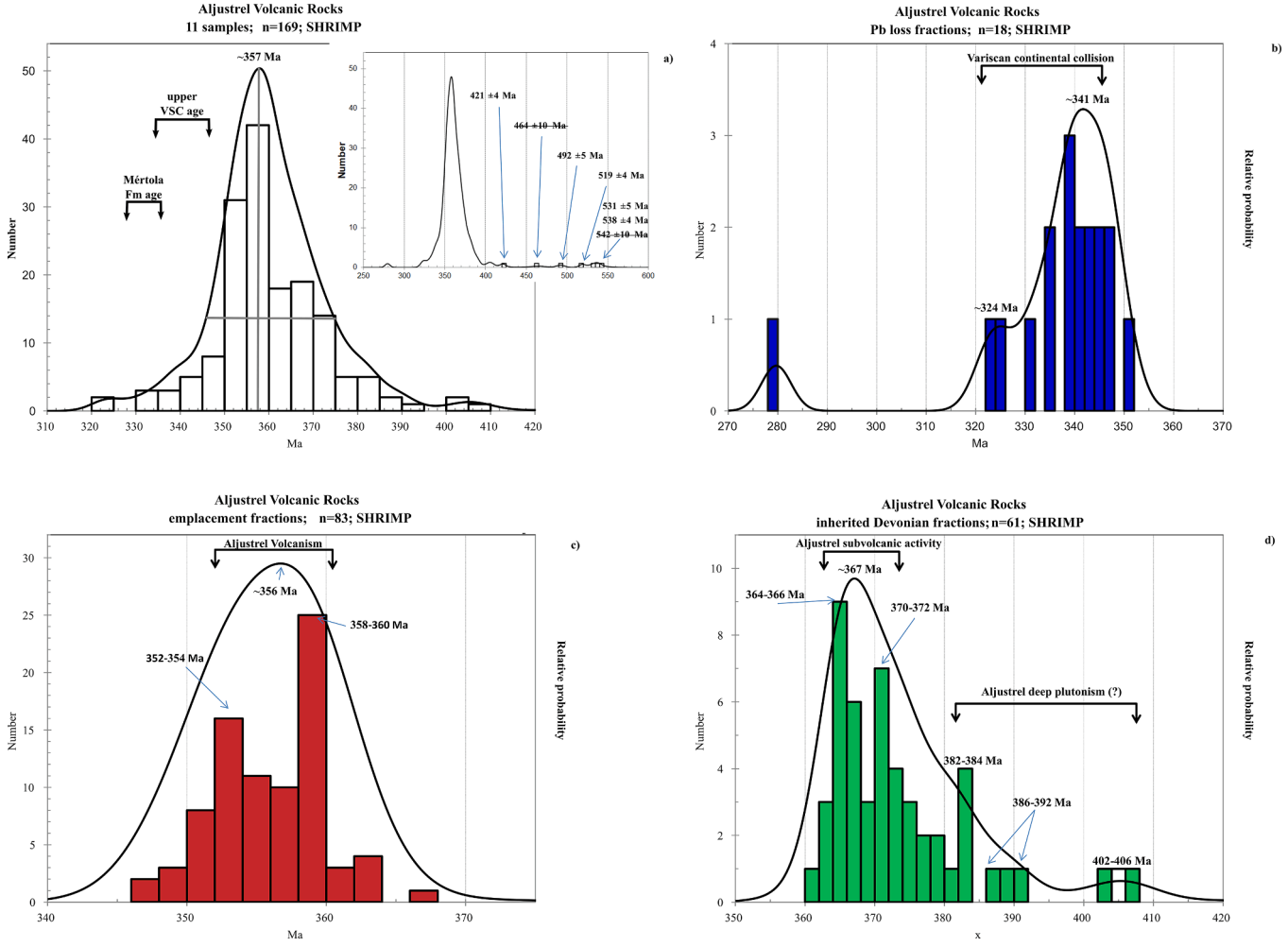

Fig. 8. Probability density plots: a) all U-Pb SHRIMP analyses with a peak at ~357 Ma; slight asymmetrical curve; b) Pb loss fractions; Variscan Orogeny 324–341 Ma (see text); c) emplacement fractions: near-symmetrical; main peak and higher bars are in agreement with obtained Concordia ages (~353–359 Ma) for volcanism (see text); d) inherited fractions: asymmetrical curve. Higher bars are roughly coincident with calculated main inherited magmatic events: ~365 Ma; ~373 Ma; ~380 Ma; ~388 Ma and ~405 Ma (see text). Note that excluded analyses 279.7 ± 3.0 Ma, 366.5 ± 4.1 Ma and 405.1 ± 21.8 Ma are included in histograms b) or d). Upper VSC age and Mértola Fm age are according to the palynostratigraphic studies in the Aljustrel Mine (Matos et al., 2010).

relative discordance (−0.3 to −19%). Thus, it is likely that some of the in-situ measurements may have resulted of Pb gain, in particular intra-grain radiogenic Pb enrichment forming nanoscale or microscale radiogenic Pb-enriched domains (Ge et al., 2019). This is consistent with the more frequent reverse discordance in the SHRIMP and LA-ICP-MS U-Pb analyses than in ID-TIMS. For whole-zircon dissolution methods, such as ID-TIMS, intra-grain Pb gain and intra-grain Pb loss sectors could balance off (Ge et al., 2019; Valley et al., 2014). Enrichment in Pb can have implications in the U-Th-Pb calculation ages. In fact, $^{206}Pb/^{238}U$ ages of grains #9.1 and #8.1 with very high discordances of sample GS18003-571 are most likely biased due to significant Pb gain (see Section 6.6). Re-heating and high-temperatures may favour intra-grain radiogenic Pb mobility into rich domains (Peterman et al., 2016; Valley et al., 2014) and low-temperature fluid-related recrystallization may also form rich Pb clusters (Ge et al., 2019). In the former scenario, it is possible that the new age resultant from post-crystallization processes (e.g. by a coupled dissolution–reprecipitation re-equilibrium mechanism; as in Geisler et al., 2007) may represent the age of the new heat event (i.e., a resetting age), thus not having implications in the calculated age fractions. Nonetheless, both mechanisms are plausible to have occurred in the Aljustrel district, as zircon grains were reheated by several magmatic events for up to 50 Ma (see Section 6.4) and later affected by hydrothermal fluids. In fact, metamictic zones (e.g. #3 GS18003-571; Fig. A11), radial cracks in fine oscillatory zoning rims into dark metamictic core (e.g. #6 FS19001-182.5; Fig. A1), diffuse zoning (e.g. #1 MM160015-168; Fig. A9), ghost zoning (#9 PM15001-521.3; Fig. A8), thick oscillatory zoning (e.g. #4 FS17004-327.8; Fig. A2), different zoning patterns (#8 FS17004-327.8), contorted zoning (e.g. #23 ES16005-635; Fig. A4), unzoned disrupted rims (#12 and 15 ES16005-620.2; Fig. A3), re-equilibrium textures (e.g. # 5 JS15001-407; Fig. A10), inverted age zoning and common inner fractures may reflect a complex post-crystallization and post-emplacement history. Furthermore, the presence of zircon grains with inverted and normal age zoning (e.g. grains #8 and #13 in Fig. A6) may suggest that post-crystallization and post-emplacement disturbance of the radiogenic isotopes were not homogenous, affecting either the outer zones or the core areas (see also Rodríguez et al., 2019), particularly if the grains were fractured (Xu et al., 2012). Incomplete resetting ages may also have contributed to the observed age variations (Bomparola et al., 2006).

The majority of Pb loss fractions have common $^{206}Pb_c$ values above 1% and $^{207}Pb/^{235}U$ σ errors above 5%. However, they often show concordance between 90 and 110% (Table 2). In this regard, we may speculate that the main age peaks and spectrum of the concordant Pb loss grains (Fig. 8b), ~324–341 Ma, of which were obtained Concordia ages between ~333–345 Ma (Table 3), most likely have a geological meaning. Thus, these younger ages may have resulted from the main deformation event related to the Variscan Orogeny (see also Paslawski et al., 2020), which is mostly coincident with the middle-late Visean depositional age (Matos et al., 2010; Rodrigues et al., 2015) of the Mértola Formation – a foreland flysch succession that materializes the main continental collision event. Moreover, zircon ages between ~330–340 Ma are well documented in Ossa-Morena Zone related to the main Variscan orogenic events (Ribeiro et al., 2019).

6.2. Emplacement ages of the volcanic rocks

In this work, 10 samples provided emplacement Concordia ages between 353 and 359 Ma, suggesting a timespan of 6 Ma for volcanism in this district (Figs. 5–7). The obtained single age error (σ) of each individual age result is relatively high when compared to Barrie et al. (2002)'s ID-TIMS single age errors and slightly lower than Rosa et al. (2009)'s LA-ICP-MS single age errors, which can produce Concordia ages from large single age ranges. Even so, SHRIMP can be a very powerful tool in complex settings, such as the Aljustrel district: 1) it is less sensitive to the effect of hydrothermal overprint in zircon (e.g. common Pb in micro-fractures and Pb loss; Tichomirowa et al., 2019) and to the presence of inclusions, which is common in the zircons of the IPB (Barrie et al., 2002), than LA-ICP-MS, because SHRIMP analyses a much smaller volume of sample; 2) SHRIMP can identify growth ages in zircon crystals, while ID-TIMS retrieves mixing ages with no geological significance.

As a control measure to validate the emplacement ages, the selected cluster of zircons had to give acceptable MSWD values at one sigma, both in the Concordia and weighted average calculations, which, for our number range of analysis used to obtain the emplacement ages (n = 5–12), is between 0.4 and 1.6 X^2_{red} (Spencer et al., 2016). In the Concordia age calculations, the MSWD of concordant zircons is too low and, therefore, MSWD and probability values presented in this work are for concordant plus equivalent zircons as suggested by Ludwig (2012). The probability for Concordia ages is frequently high (>80%) and for weighted average ages is, however, quite variable (0.9–99%). The MSDW obtained for the Corcordia ages can be significantly different from weighted average ages (e.g. 0.46 and 0.91, respectively for sample FS19001-182.5). Still, Concordia ages were commonly obtained from single ages ranging ~10 Ma (e.g. 351–360 Ma, FS17019-182.5; 350–366 Ma, GS18003-571; Table 2) and, more relevantly, the age range of the zircons used to obtain the emplacement age of each sample overlaps, although providing distinct Concordia ages (353–359 Ma). Thus, it is reasonable to ponder if the different Concordia ages are in fact related to distinct magmatic events and/or related to analytical deviations from a rather homogenous zircon population (see Spencer et al., 2016; Rodríguez et al., 2019; Tichomirowa et al., 2019 and references therein) or even Pb mobility (see discussion in Section 6.1). However, Barrie et al. (2002)'s and Valenzuela et al. (2011)'s ID-TIMS results, strongly suggest that, at least in the Rio Tinto area, several magmatic pulses may have occurred at least separated by only ~2 Ma. This time span possibly represents the resolution of the technique coupled with the small number of analyses. Actually, the magmatic batches could have been generated in shorter periods. Nonetheless, we should notice that ID-TIMS is more prone to mixture different zircon ages in complex grains but is also less sensitive to inter-grain Pb mobility. In the IPB and in particular in mining areas such as Aljustrel, we may expect a similar behaviour of Rio Tinto magmatism (Valenzuela et al., 2011). This might suggest that the single age variation of the emplacement fractions of our samples is a mixture of intrinsic errors of analytical techniques and intrinsic geological variation, which are obviously difficult, if not impossible, to quantify with the current data. The problem falls into the significance of the calculated emplacement ages: if multiple magmatogenic events incorporated older zircon crystallization events does the Concordia age represent the emplacement age? Or should we consider the younger single age fractions as the emplacement age? There are good examples of this problem, wherein the emplacement weighted average diagrams (see supplementary data 2) it is possible to observe different clusters at slightly different ages. For example, in sample FS19001-182.5 a cluster at ~351 Ma is distinguishable from another cluster at ~357–358 Ma (Fig. B6) and in sample GS18003-571 it is possible to individualize three clusters at ~348 Ma, ~353 Ma and ~359 Ma (Fig. L4). In addition, in AS18003-359.3 sample, emplacement fractions have so remarkable graphical distinction that alternative ages are presented (Table 3). In the probability density plot of the emplacement fractions (Fig. 8c), the ~353 Ma and ~359 Ma zircons are the best represented with a peak at ~356 Ma, which could also suggest multiple magmatic events. In addition, the morphology of grain #5 in hole GS18003-571 (Fig. A11) could actually suggest the presence of two-stage crystallization processes (i.e. overgrowth) with a younger (~350 Ma) event crystalizing around an older zircon (~359 Ma). Thus, the best approach is to consider that the calculated Concordia ages represent maximum ages of emplacement.

Taking the discussion above, we suggest that the volcanism in Aljustrel occurred in the period between 359 and 353 Ma (Fig. 8c), which was responsible for the thick volcanic succession in the area.

Abundant volcanism may suggest a rather shallow emplacement of magma chambers (<1.5–2.5 kbar; Huber et al., 2019), which could be related to asthenospheric upwelling and subsequent crustal uplift. However, volcanism from deep sources is not excluded, as almandine garnets (Barriga and Fyfe, 1997) of the unmineralized Megacrystal Volcanic Unit may imply. Thus, we suggest possible concomitant shallower sourced (353–355 Ma; mineralized Mine Volcanic Unit) and deeper sourced volcanism (~355 Ma; barren Megacrystal Volcanic Unit). Deep magma chambers are not incompatible with an igneous origin for the feldspar megacrysts (Eklund and Shebanov, 2005). In fact, effusive silicic melts with megacrysts require a rapid ascent, as the presence of igneous almandine also could suggest (Sieck et al., 2019). Nonetheless, a hydrothermal origin, based on mineral chemistry results, was previously suggested (Barriga, 1983).

Furthermore, we speculate that the present geochronological work coupled with previous ID-TIMS studies (Barrie et al., 2002) suggest that volcanism in the Aljustrel district is marked by multiple events which incorporate zircons from the previous events. Therefore, we have assumed that only maximum emplacement ages can be obtained. These maximum ages open the possibility that the last pulses of volcanic activity and subsequent deposition of the massive sulphides were diachronic in the different Aljustrel sub-basins.

6.3. Age of the massive sulphides

The age of the massive sulphides must be constrained by the youngest coherent or autoclastic volcanic rocks immediately below or above the massive sulphides, considering a brine pool model for the deposition of the Aljustrel massive sulphides (Inverno et al., 2008).

The maximum age for deposition of Feitais massive sulphides is constrained by sample FS17019-182.5, collected ~5 m below the massive sulphides (Fig. 2), which provided an age of 354.6 ± 2.3 Ma.

Estação massive sulphides should have been well constrained with the two samples collected above and below the massive sulphides. However, sample ES16005-620.2 collected within the cherts provided an older age than the one obtained in sample ES16005-635, which provided an age of 354.9 ± 1.9 Ma (Fig. 2). This is the best age estimate for Estação massive sulphides. Both Feitais and Estação deposits have been considered the same sulphide lens disrupted by later faults; the maximum precipitation ages of both deposits further support such interpretation.

At Algares deposit, the maximum age of massive sulphide deposition is given by sample AS18005-359.5, collected 5 m below the massive sulphide lens (Fig. 2), which provided an emplacement age of 358.2 ± 2.8 Ma. However, the crystal-rich level collected near the Algares gossan by Barrie et al. (2002) suggests an age of the massive sulphides of 352.4 ± 1.9 Ma, based on 4 grains, which is further supported by sample AS18007-436 collected ~60 m below the massive sulphide lens that provided an emplacement age of 353.3 ± 2.4 Ma. (Table 3; Fig. 2). Thus, the best age estimate for Algares sulphides is ~353 Ma.

At Moinho, the maximum deposition age of massive sulphides is given by sample MM16015-168, affected by stockwork mineralization, with an emplacement age of 358.9 ± 2.0 Ma.

At São João, zircons obtained in sample JS15001-407 were interpreted as inherited, which provides a much older maximum deposition age of 364.4 ± 2.1 Ma for massive sulphides of the São João deposit. Both Moinho and São João deposits are heavily faulted, implying that the relationship between the massive sulphides and volcanic flows is difficult to establish. However, São João and Moinho have been considered as part of the same massive sulphide lens and, thus, a similar maximum deposition age of the Moinho deposit should be assumed for São João as well.

Massive sulphides of Gavião deposit have a maximum deposition age of 356.3 ± 2.0 Ma. This age was obtained in GS18003-571 sample that was collected ~14 m below the massive sulphides in a strongly altered stockwork zone.

Maximum deposition ages of the massive sulphides in the Aljustrel district suggest that the Algares deposit is the youngest one (~353 Ma); Feitais-Estação and Gavião deposits are slightly older (~355 and 356 Ma, respectively) and São João and Moinho deposits are the oldest ones (~359 Ma). This may suggest that magmatic centres and magmatic cessation in the Aljustrel district were not contemporaneous along the basins. Apparently, western sectors are older than eastern sectors. Furthermore, the difference between the maximum deposition age of São João and Gavião suggests that these deposits were formed in different basins and are not part of the same lens displaced by the Messejana Fault, as had previously been suggested (Andrade and Schermerhorn, 1971). This opens exploration potential on both sides of the Messejana Fault, for finding the continuation of Gavião and São João massive lenses (see also Relvas et al., 2011).

6.4. Devonian inherited ages of the Aljustrel district

In the Aljustrel district, inherited fractions were commonly analysed (~40% of the total amount), occasionally representing>50% of the zircons analysed in a single sample (e.g. sample AS18005-359.5).

The youngest inherited fractions that are clearly separated from the emplacement fractions can be found in samples ES16005-635, FS17004-327.8, AS18007-436 and MM16005-168 with the following Concordia ages: 373.4 ± 3.4 Ma; 365.7 ± 4.3 Ma; 367.3 ± 4.1 Ma and 369.9 ± 5.5 Ma, respectively (Table 3; Figs. 5–7; Fig. D2, C4, F2 and J2). These ages practically define the most relevant timespan for inherited fractions (364–373 Ma). In these samples, the gap between the youngest single age of the main inherited fraction and the oldest single age of the emplacement fraction is 6 to 10 Ma. In samples AS18003-359.3, AS18007-436, ES16005-620.2, FS17004-327.8 and MM16015-168 more than one inherited fraction is clearly visible. The inherited ages identified in this work are well-defined by spots or Concordias with absent or low content of grains with $^{206}Pb_c > 1\%$, $^{207}Pb/^{235}U\ \sigma > 5\%$ and/or discordance >|10%| (see underlined ages in Table 3). For some samples it is rather difficult to establish a difference between the inherited fraction and the emplacement fraction. For instance, in sample ES16005-620.2 there is a clear σ error overlapping in the Concordia diagram (Fig. 5c, D2) between the emplacement and inherited fractions, which is enhanced by the presence of grains with higher errors (labelled as blue in Fig. D2). In this sample, the single $^{206}Pb/^{238}U$ age gap between emplacement and inherited single ages is ~4 Ma. Actually, a well-defined Concordia is possible to obtain adding the youngest inherited grains to the emplacement grains, which would had resulted in an emplacement Concordia age of 360.9 ± 1.9 Ma with a MSWD = 0.9 (not shown). However, the weighted average age would had resulted in an age with a MSWD = 1.8 (not shown), which is at the edge of the acceptable X^2_{red} values at 2σ level for 13 grains (Spencer et al., 2016). We have assumed that 1σ level, in both weighted average and Concordia calculations, is more accurate for the larger single age variability of these rocks. In addition, the 6 grains that were added to the emplacement fraction in this exercise have a very small single age variation (364–366 Ma; Fig. D4). These are coeval to the already identified inherited fraction in other samples where the gap between emplacement and inherited fractions is wider and clearer (see above). However, occasionally, a graphical approach was also used. For example, in the same sample ES16005-620.2, it was possible to graphically separate the inherited fraction (364.7 ± 2.6 Ma; n = 6) from another inherited fraction (370.1 ± 4.2 Ma; n = 3) (Fig. D4). However, Concordia and weighted average ages of both inherited fractions would have resulted in an acceptable MSWD value of 0.62. Thus, slight variations in age of the inherited fractions between samples, particularly those with higher content of "blue grains" (see Appendix A), might have resulted of the options taken to calculate the Concordia ages, lack of statistically relevant number of spots for those Concordia ages and internal geological variation, considering the possibility that the time interval between magma pulses was in the order of a few million years. Single age

fractions were also important to define several inherited fractions.

Another used approach was the analysis of the probability density plot. The continuous, ~20 Ma, single age variation between 360 and 383 Ma of the entire SHRIMP dataset (Fig. 8a), may suggest that more than one magmatic event occurred during this period. Single age gaps of 5 Ma and 14 Ma define small clusters at ~388 Ma and ~405 Ma (Table 2). According to our calculations (Table 3) inherited fractions between ~364 and ~383 Ma are characterized by multiple crystallization events apart from each other by only a few millions years. Furthermore, if we only plot the inherited fractions, it results in a clearly asymmetrical probability density curve (Fig. 8d) with a peak at ~367 Ma and a residual peak at ~405 Ma, showing that between ~367 and ~405 Ma there was at least more than one crystallization event.

Several Devonian inherited fractions have also been recently identified in the Neves-Corvo volcanic rocks (Albardeiro et al., 2019; Oliveira et al., 2013; Pereira et al., 2014; Solá et al., 2015). Due to these findings, these authors suggested a long-term magmatic activity in that region. In the Aljustrel region, a possible link between volcanism and PQ Formation has been previously suggested (Rosa et al., 2009). So, we may question if the Devonian zircons found in the Aljustrel volcanic rocks could have been derived from the PQ Formation.

So far, no zircons younger than ~413 Ma have been found in the PQ quartzites of the western sectors of the IPB where Aljustrel is located (Braid et al., 2011; Pereira et al., 2012; Rosa et al., 2009). Upper Devonian fractions were only found in metagreywackes of the PQ Formation at the easternmost sector of the IPB (Pérez-Cáceres et al., 2017). However, even if we consider that U-Pb zircon data of PQG, in the western sectors, is still scarce and, therefore, the Middle to Upper Devonian PQ Formation could have provided the Devonian zircons, it would imply magmatogenesis or abundant crustal assimilation at extremely shallow depths, assuming the current thickness estimate for the known PQG formations (~2 km; ≪1 kbar). So far, no evidence was found for such a shallow melting or emplacement: shallow melting depths would imply a substantial higher metamorphic grade than the low metamorphic facies identified in the IPB (Munhá, 1990), and the only record of plutonism in the IPB (Sierra Norte Batholith) intrudes in the known PQG rocks during the Visean (~340–343 Ma), post-dating the main VSC activity (Paslawski et al., 2020). Furthermore, the known PQ of the eastern sectors of the IPB that contains Upper Devonian populations is still characterized by abundant Proterozoic ages (>70%). Thus, the residual Proterozoic inheritance (see Rosa et al., 2009 and Section 6.6) when compared to the well-represented Upper Devonian inheritance in the Aljustrel district strongly suggests that these latter fractions were not derived from known siliciclastic rocks. In addition, as previously mentioned, poor-Mn almandine garnets found in the unmineralized Megacrystal Volcanic Unit, which were interpreted to be of magmatic origin (Barriga, 1983; Barriga and Fyfe, 1997), could suggest rapid magma ascent from deep magma chambers (Sieck et al., 2019). Thus, the occurrence of several Devonian zircon populations in the barren Megacrystal Volcanic Unit (the oldest is ~384 Ma) implies that Upper Devonian to uppermost Middle Devonian inheritance should not have been derived from the melting of the known PQG rocks. Therefore, older unknown (cryptic) basement rocks are a more likely crustal source for the volcanic rocks of Aljustrel, such as the thick segments identified in seismic profiles at upper- and mid-crustal levels (Schmelzbach et al., 2008; Simancas et al., 2003).

Thus, we suggest that early magmatism in the Aljustrel district started at ~405 Ma and that another magmatic event occurred at 388 Ma and at 380 Ma (Fig. 8d). These events, of which the Middle and Lower Devonian are poorly represented, could be plutonic or represent small partial melting events, although an origin for the Lower Devonian fractions from a siliciclastic source beneath the known PQG of at least ~388 Ma cannot be entirely discharged. Increasing of magmatic activity in the Upper Devonian has its uttermost expression with the beginning of volcanism in the IPB in the Cercal area (Rosa et al., 2009), which is also recorded in several areas of the IPB (e.g. Oliveira et al., 2013) as in the Aljustrel district by the presence of significant inherited zircon populations. Thus, we may postulate that during the Upper Devonian, magmatism in the IPB, and in particular in the Aljustrel district, was probably dominated by non-extrusive sub-volcanic magma chambers below the known PQ (>2.5 kbar; Huber et al., 2019). In the Aljustrel district, at least two main inherited magmatic events were identified at 373 Ma and at 365 Ma (Fig. 8d). The later event is the most important inherited magmatic event, just 6 Ma apart from the beginning of the main Aljustrel volcanism, which suggests that non-extrusive sub-volcanism extended until at least 365 Main this region. In addition, as will be discussed in Section 6.5 ahead, based on Th/U ratios, it was also possible to identify cryptic mafic magmatism related to the youngest inherited event. Thus, and considering the inherited character of these high Th/U grains, mafic rocks may have also been remelted in later felsic events, suggesting a rather complex crustal source (with multiple sources at different crustal levels) and crustal assimilation. Interestingly, minor mafic volcanism is concomitant with felsic volcanism in the Gavião and Algares deposits (Fig. 2), and, according to Leitão (2009), also post-dates it, in the Aljustrel's mine lease area.

These magmatic events taken together imply a time span of about 50 Ma for the magmatic activity in the Aljustrel district (~353 – see Section 6.2 – to ~405 Ma), which is in agreement with the hypothetically ~60 Ma timespan in the Neves-Corvo area (Solá et al., 2015). In addition, we may postulate that the seismic reflective bodies identified at mid and upper crustal depths beneath the SPZ and interpreted as igneous intrusions (Palomeras et al., 2011; Schmelzbach et al., 2008) could reflect an unknown subvolcanic and plutonic activity in the IPB formed during this long-term magmatic period.

6.5. Th/U ratios and significance of JS15001-407 zircons

Th/U ratios of the emplacement and Devonian inherited fractions and those grains which have experienced Pb loss are rather similar. No relationship was observed between age fractions and Th/U ratios. Excluding JS15001-407 main Concordia grains, which have anomalous Th/U ratios, Devonian and Carboniferous zircons present Th/U ratios mostly comprised between 0.4 and 0.9 (interquartile range), averaging 0.7 ± 0.3 and ranging between 0.0 and 1.8. However, lower Th/U ratios are often related to low Th content, which in turn is also often associated with higher $^{206}Pb/^{238}U/^{208}Pb/^{232}Th$ discordance. By removing zircons with Th < 100 ppm and with $^{206}Pb/^{238}U/^{208}Pb/^{232}Th$ discordance > |10|%; the interquartile range of the 94 spots becomes 0.5–1, with an average of 0.8 ± 0.3 and a range of 0.3–1.8. Therefore, it is possible that very low Th/U ratios (<0.3) may represent disturbance of Th or co-crystallization with allanite, which has been previously identified in Aljustrel (Barriga and Fyfe, 1997). The remaining 54 spots, with low Th or high discordance, have an interquartile range of 0.5–0.6, averaging 0.5 ± 0.2 and ranging between 0.0 and 1.3. Nonetheless, both aforementioned averaging ratios show Th/U ratios above 0.5, which are common values found in zircons of igneous origin (Hoskin and Schaltegger, 2003).

Th/U ratios depend on several factors, such as the temperature of crystallization, the initial ratio in the melt, precipitation of Th or U-rich cogenetic minerals (allanite, monazite, xenotime, etc.) and crystal growth rate (Kirkland et al., 2015; Siégel et al., 2018; Wang et al., 2011).

Some grains that were incorporated in the same Concordia calculations show decreasing of Th/U ratios from core to rim (see Table 2). For example, in grain #13 of sample AS18005-359.5, Th/U decreases from 1.1 (~356 Ma) to 0.6 (335 Ma; which has experienced Pb loss). In grain #8 of the same sample, Th/U decreases from 0.8 (~346 Ma; which has experienced Pb loss) to 0.5 (~359 Ma). For sample GS18003-571, in grain #2 Th/U decreases from 0.9 in its core (~361 Ma) to 0.7 (~354 Ma; which is $^{206}Pb/^{238}U/^{208}Pb/^{232}Th$ discordant) in its rim; in grain #3 Th/U decreases from 1 (~345 Ma, which has experienced Pb loss) to 0.7 (~353 Ma) and in grain #5 decreases from 0.7 (~359 Ma) to 0.4 (~350 Ma). Allanite, which has been identified in the Aljustrel volcanic rocks

(Barriga and Fyfe, 1997), may explain the very low Th content (<100 ppm) and Th/U (<0.3) ratios in some spots, but would not explain higher Th content and Th/U ratios at the rims in these zircons (e.g. #11.2 Th/U = 0.6 and Th = 164 ppm; FS19001-182.5). Thus, and considering the fact that the constant decreasing of the Th/U ratios from the core to the rim observed in the Aljustrel zircons is independent of Pb loss (e.g. #8 AS18005-359.5 and #6 FS19001-182.5), we suggest that, for the emplacement fractions, zircon rims grew in a more fractionated magma and of lower temperature than from the zircon cores, whether they grew from the same magma batch or not.

In addition, to test the equilibrium between the Th/U in zircon with a melt of similar composition with the whole-rock data, we estimated the $Th_{(zircon/rock)}/U_{(zircon/rock)}$. Uranium is a mobile element under seawater hydrothermal circulation and, therefore, caution is required for the following approach. Kirkland et al. (2015) developed an "equilibrium line" between $Th_{(zircon/rock)}/U_{(zircon/rock)}$ and temperature based on a large dataset of igneous rocks. If crystals are plotted below that line zircons may have formed in a more fractionated magma than reported in the whole-rock. However, if plotted above that "equilibrium line" the zircon crystals may have formed in a less fractionated magma than the whole-rock (Kirkland et al., 2015). According to Kirkland et al. (2015), this ratio coupled with zircon temperature can identify antecrysts. However, in general, no relationship can be seen between zircon age fractions and $Th_{(zircon/rock)}/U_{(zircon/rock)}$ (see also Siégel et al., 2018). Considering that temperatures obtained in the volcanic rocks of the IPB by Ti-in-zircon and quartz-hosted melt inclusions are in excess of 700–800 °C (Marques et al., 2020; Mello, 2020), and assuming this as a reference temperature for equilibrium between zircon and melt, the expected $Th_{(zircon/rock)}/U_{(zircon/rock)}$ ratio is ~0.6–0.4. For higher temperatures the ratio decreases (Kirkland et al., 2015). Most samples, indeed, provided $Th_{(zircon/rock)}/U_{(zircon/rock)}$ values below 0.4. Overall, this suggest that, independently of U gain or loss in the rock by hydrothermal alteration, the zircons may have crystalized from an equally or more fractionated melt than materialized by the whole-rock. Thus, inherited Devonian zircons are most likely derived from felsic rocks.

However, samples FS17004-327.8 and JS15001-407 provided higher $Th_{(zircon/rock)}/U_{(zircon/rock)}$ average ratios (~1 and 0.8, respectively). The former has high contents of U (~25.9 ppm) suggesting U gain, and, therefore, no more considerations will be made. The latter may suggest that zircons may have formed in a less fractionated melt (or in a melt with a temperature below 700 °C, assuming crystallization in equilibrium with the melt). This sample has Th/U ratios in zircon averaging 2.1 ± 1.7. Th/U ratios in zircon above 1 are more common in mafic suites (Heaman et al., 1990) and rare in felsic rocks (Wang et al., 2011). Thus, high Th/U ratios in zircons of JS15001-407 sample strongly suggest a mafic source at ~365 Ma, which reinforces that the Concordia age obtained in this sample is an inherited age (see Section 5.2.10). It is worthwhile mentioning that in this sample the youngest fractions have a tendency for higher Th/U and $Th_{(zircon/rock)}/U_{(zircon/rock)}$ than the older fractions, which may suggest mixing from different sources.

Considering Th/U ratios in zircons, Aljustrel volcanic rocks may have been formed from melts generated from different sources, which not only included felsic magmatic rocks ($Th_{(zircon/rock)}/U_{(zircon/rock)} < 0.4$ in inherited fractions), but also mafic-intermediate magmatic rocks (high Th/U and $Th_{(zircon/rock)}/U_{(zircon/rock)}$ ratios in inherited fractions), which are typical sources for metaluminous felsic rocks. In addition, other unknown sources were also important as indicated by pre-Devonian inherited zircons (see below).

6.6. Pre-Devonian fractions and unknown basement sources

The pre-Devonian fractions represent only 4% of the grains analysed in this work, and, as in Barrie et al. (2002), only Phanerozoic pre-Devonian fractions were identified. On the other hand, in Rosa et al. (2009), only Neoproterozoic and Archean pre-Devonian fractions were identified. In previous Section 6.4. we concluded that it is unlikely that melting or magma chamber emplacement occurred in the known PQG, thus, pre-Devonian zircons were attributed to an unknown basement. However, caution is needed, as the oldest known rocks in the IPB, the PQG, are discerned by their high contents of pre-Devonian zircon ages (e.g. Braid et al., 2011) and contamination from this group during melt ascent cannot be excluded.

Phanerozoic pre-Devonian grains are often concordant to slightly negative discordant (−2.3% to −12.6%) and two grains are highly negative discordant (−77%; −61%). These two highly negative discordant ages of sample GS18003-571 with middle Ordovician and lower Cambrian apparent ages probably represent intra-grain Pb gain (see Section 6.1) and, therefore, these grains cannot be considered. Unfortunately, it was not possible to model these grains back to the Concordia. Thus, Phanerozoic pre-Devonian grains are given by samples AS18007-436; ES16005-635, FS17004-327.8 (this work), 98TB007 (Barrie et al., 2002), SJ1 and FEV1 (Rosa et al., 2009) in which were retrieved: an uppermost Silurian grain (421.1 ± 7.6 Ma) and the well-represented Cambrian ages (5 grains: 492.1 ± 10.2 Ma; 518.8 ± 8.0 Ma; 528.9 ± 3.3 Ma, 531.2 ± 10.4 Ma and 537.9 ± 8.4 Ma). Early Cambrian grains, which are represented in minor quantities in the PQG rocks (<4%), are an important inherited fraction in the Aljustrel district. Likewise, Neoproterozoic ages are well represented in this district (543 ± 8 Ma; 594 ± 16 Ma; 596 ± 8 Ma; 609 ± 8 Ma; 634 ± 18 Ma; Rosa et al., 2009). An Archean grain (2640 ± 10 Ma) was also retrieved by Rosa et al. (2009).

In comparison with other districts in the IPB, Aljustrel volcanic rocks together with Neves-Corvo (Pereira et al., 2014) are, so far, the only districts containing lower Cambrian zircons. Although, one lower Cambrian zircon had already been identified (Barrie et al., 2002), in this work we were able to confirm, with two more analyses, that the presence of lower Cambrian zircons is a significant pre-Devonian population in the Aljustrel district (Fig. 8a), which together with the late Silurian age, obtained in this work, and the Neoproterozoic and Archaean grains recovered by Rosa et al. (2009) can bring new implications for the paleogeographic evolution of the South Portuguese Zone.

7. Conclusions

The main conclusions of the U-Pb SHRIMP geochronological results of the volcanic rocks hosting the economic mineralization of Aljustrel Mine and the Gavião near-mining exploration project are:

1) Lower Carboniferous volcanic rocks of the Aljustrel district contain abundant records of previous geological events from the Archaean to late Devonian. Early Carboniferous inheritance cannot be entirely excluded.
2) Devonian and Carboniferous zircons may imply that the magmatic activity in the Aljustrel district was present during ~50 Ma. Accordingly, apparent main magmatic events identified in this work are: a) 405 Ma, 388 Ma and 380 Ma, that hypothetically may represent deep plutonism or other melting episodes; b) 373 Ma and 365 Ma, plausibly representing non-extrusive subvolcanic activity; and c) 353–359 Ma main extrusive volcanic activity materializing shallower subvolcanic activity and possibly deep source-related magma chambers.
3) At ~373 Ma, the Aljustrel district is marked by an increase of magmatic activity, which is coincident with the oldest known volcanic rocks of the IPB.
4) High values of Th/U ratios in zircons of sample JS15001-407 suggest zircon precipitation in a mafic composition melt at ~364 Ma.
5) The volcanic pile (>250 m) in the Aljustrel district was emplaced between 353 and 359 Ma.
6) Maximum emplacement ages in the different deposits of Aljustrel may suggest a diachronic massive sulphide deposition.
7) A Pb loss event (~324–345 Ma) was responsible for the U-Pb disturbance and resetting of magmatic zircons, most likely associated with the Variscan Orogeny.

8. Research data for this article

Data will be made available on request.

Declaration of Competing Interest

The authors declare that they have no known competing financial interests or personal relationships that could have appeared to influence the work reported in this paper.

Acknowledgements

We acknowledge the support of FCT through PhD grant SFRH/BD/138791/2018 to João Lains Amaral and through project UIDB/50019/2020 to IDL – Instituto Dom Luiz. João Lains Amaral strongly appreciates all the CPGeo-IG-USP/GeoLab-SHRIMP staff work and support, particularly Kei Sato, Artur Onoe, Nayara Silva, Daniela Silva and Silvana Macedo. He also acknowledges Carlos Rosa for the helpful discussion on the Aljustrel's volcanic facies. We would also like to thank Luís Albardeiro for constructive discussions in the early stages of the manuscript and Ezequiel Ferreira for helping in zircon separation. This is a contribution to the research project PetroGeo (LNEG). The two anonymous referees are acknowledged for valuable comments that improved the manuscript.

Appendix A. Supplementary data

Supplementary data to this article can be found online at https://doi.org/10.1016/j.oregeorev.2021.104147.

References

Albardeiro, L., Morais, I., Solá, R., Salgueiro, R., Matos, J., Oliveira, D., Pacheco, N., Araújo, V., 2019. Deciphering U-Pb ages in zircon from Volcano-Sedimentary Complex felsic volcanic rocks. Examples from the Neves-Corvo mining District, Iberian Pyrite Belt, Portugal. In: Geophysical Research Abstracts, EGU General Assembly 2019, 21. pp. EGU2019-15330.

Andrade, R.F., Schermerhorn, L.J.G., 1971. Aljustrel e Gavião. In: Carvalho, D., Goinhas, J.A.C., Schermerhorn, L.J.G. (Eds.), Principais Jazigos Minerais Do Sul de Portugal. Direcção-Geral de Minas e Serviços Geológicos, Lisboa, pp. 32–59.

Barrett, T., 2008. Chemostratigraphy, Petrography and Alteration of Volcanic Rocks at the Feitais Deposit and in Two Regional Holes, Aljustrel Area, Portugal. Unpublished report for AGC Minas de Portugal Unipessoal Lda, pp. 33.

Barrett, T.J., Dawson, G.L., MacLean, W.H., 2008. Volcanic stratigraphy, alteration, and sea-floor setting of the Paleozoic Feitais Massive Sulfide Deposit, Aljustrel, Portugal. Econ. Geol. 103 (1), 215–239. https://doi.org/10.2113/gsecongeo.103.1.215.

Barrie, T.C., Amelin, Y., Pascual, E., 2002. U-Pb Geochronology of VMS mineralization in the Iberian Pyrite Belt. Miner. Depos. 37 (8), 684–703. https://doi.org/10.1007/s00126-002-0302-7.

Barriga, F., 1983. Hydrothermal Metamorphism And Ore Genesis At Aljustrel. Unpublished PhD. University Ontario, Canada, Portugal, p. 368.

Barriga, F.J.A.S., Fyfe, W.S., 1997. Multi-phase water-rhyolite interaction and ore fluid generation at Aljustrel, Portugal. Miner. Depos. 33 (1-2), 188–207. https://doi.org/10.1007/s001260050140.

Barriga, F.J.A.S., Fyfe, W.S., 1988. Giant pyritic base-metal deposits: the example of Feitais (Aljustrel, Portugal). Chem. Geol. 69 (3-4), 331–343. https://doi.org/10.1016/0009-2541(88)90044-7.

Black, L.P., Kamo, S.L., Allen, C.M., Aleinikoff, J.N., Davis, D.W., Korsch, R.J., Foudoulis, C., 2003. TEMORA 1: a new zircon standard for Phanerozoic U-Pb geochronology. Chem. Geol. 200 (1-2), 155–170. https://doi.org/10.1016/S0009-2541(03)00165-7.

Black, L.P., Kamo, S.L., Allen, C.M., Davis, D.W., Aleinikoff, J.N., Valley, J.W., Mundil, R., Campbell, I.H., Korsch, R.J., Williams, I.S., Foudoulis, C., 2004. Improved 206Pb/238U microprobe geochronology by the monitoring of a trace-element-related matrix effect; SHRIMP, ID–TIMS, ELA–ICP–MS and oxygen isotope documentation for a series of zircon standards. Chem. Geol. 205 (1-2), 115–140. https://doi.org/10.1016/j.chemgeo.2004.01.003.

Bomparola, R.M., Ghezzo, C., Belousova, E., Griffin, W.L., O'Reilly, S.Y., 2006. Resetting of the U-Pb zircon system in Cambro-Ordovician Intrusives of the Deep Freeze Range, Northern Victoria Land, Antarctica. J. Petrol. 48, 327–364. https://doi.org/10.1093/petrology/egl064.

Braid, J.A., Murphy, J.B., Quesada, C., Bickerton, L., Mortensen, J.K., 2012. Probing the composition of unexposed basement, South Portuguese Zone, southern Iberia: implications for the connections between the Appalachian and Variscan orogens. Can. J. Earth Sci. https://doi.org/10.1139/E11-071.

Braid, J.A., Murphy, J.B., Quesada, C., Mortensen, J., 2011. Tectonic escape of a crustal fragment during the closure of the Rheic Ocean: U-Pb detrital zircon data from the Late Palaeozoic Pulo do Lobo and South Portuguese zones, southern Iberia. J. Geol. Soc. London 168 (2), 383–392. https://doi.org/10.1144/0016-76492010-104.

Cohen, K.M., Finney, S.C., Gibbard, P.L., Fan, J.-X., 2013. The ICS International Chronostratigraphic Chart. Int. Union Geol. Sci. 36, 199–204. https://doi.org/10.18814/epiiugs/2013/v36i3/002.

Donaire, T., Pascual, E., Sáez, R., Pin, C., Hamilton, M.A., Toscano, M., 2020. Geochemical and Nd isotopic signature of felsic volcanic rocks as a proxy of volcanic-hosted massive sulphide deposits in the Iberian Pyrite Belt (SW, Spain): The Paymogo Volcano-Sedimentary Alignment. Ore Geol. Rev. 120 https://doi.org/10.1016/j.oregeorev.2020.103408.

Dunning, G.R., Díez Montes, A., Matas, J., Martín Parra, L.M., Almarza, J., Donaire, M., 2002. Geocronología U/Pb del volcanismo ácido y granitoides de la Faja Pirítica Ibérica (Zona Surportuguesa). Geogaceta 32, 127–130.

Eklund, O., Shebanov, A., 2005. Prolonged postcollisional shoshonitic magmatism in the southern Svecofennian domain – a case study of the Åva granite–lamprophyre ring complex. Lithos 80, 229–247. https://doi.org/10.1016/j.lithos.2004.06.012.

Ge, R., Wilde, S.A., Nemchin, A.A., Whitehouse, M.J., Bellucci, J.J., Erickson, T.M., 2019. Mechanisms and consequences of intra-crystalline enrichment of ancient radiogenic Pb in detrital Hadean zircons from the Jack Hills, Western Australia. Earth Planet. Sci. Lett. 517, 38–49. https://doi.org/10.1016/j.epsl.2019.04.005.

Geisler, T., Schaltegger, U., Tomaschek, F., 2007. Re-equilibration of zircon in aqueous fluids and melts. Elements 3 (1), 43–50. https://doi.org/10.2113/gselements.3.1.43.

Gifkins, C., Herrmann, W., Large, R., 2005. Altered Volcanic Rocks; A Guide to Description and Interpretation. Centre for Ore Deposit Research, University of Tasmania.

González, F., Moreno, C., Sáez, R., Clayton, G., 2002. Ore genesis age of the Tharsis Mining District (Iberian Pyrite Belt): a palynological approach. J. Geol. Soc. London 159, 229–232. https://doi.org/10.1144/0016-764901-142.

Hart, T.R., Gibson, H.L., Lesher, C.M., 2004. Trace element geochemistry and petrogenesis of felsic volcanic rocks associated with volcanogenic massive Cu-Zn-Pb sulfide deposits. Econ. Geol. 99, 1003–1013. https://doi.org/10.2113/gsecongeo.99.5.1003.

Heaman, L.M., Bowins, R., Crocket, J., 1990. The chemical composition of igneous zircon suites: implications for geochemical tracer studies. Geochim. Cosmochim. Acta 54, 1597–1607. https://doi.org/10.1016/0016-7037(90)90394-Z.

Herrington, R., Maslennikov, V., Zaykov, V., Seravkin, I., Kosarev, A., Buschmann, B., Orgeval, J.-J., Holland, N., Tesalina, S., Nimis, P., Armstrong, R., 2005. 6: Classification of VMS deposits: lessons from the South Uralides. Ore Geol. Rev. 27, 203–237. https://doi.org/10.1016/J.OREGEOREV.2005.07.014.

Hoskin, P.W.O., Schaltegger, U., 2003. The composition of zircon and igneous and metamorphic petrogenesis. Rev. Mineral. Geochem. 53, 27–62. https://doi.org/10.2113/0530027.

Huber, C., Townsend, M., Degruyter, W., Bachmann, O., 2019. Optimal depth of subvolcanic magma chamber growth controlled by volatiles and crust rheology. Nat. Geosci. 12, 762–768. https://doi.org/10.1038/s41561-019-0415-6.

Inverno, C.M.C., Solomon, M., Barton, M.D., Foden, J., 2008. The Cu Stockwork and Massive Sulfide Ore of the Feitais Volcanic-Hosted Massive Sulfide Deposit, Aljustrel, Iberian Pyrite Belt, Portugal: A Mineralogical, Fluid Inclusion, and Isotopic Investigation. Econ. Geol. 103, 241–267. https://doi.org/10.2113/gsecongeo.103.1.241.

Ireland, T.R., Williams, I.S., 2003. Considerations in Zircon Geochronology by SIMS. Rev. Mineral. Geochem. 53, 215–241. https://doi.org/10.2113/0530215.

Kirkland, C.L., Smithies, R.H., Taylor, R.J.M., Evans, N., McDonald, B., 2015. Zircon Th/U ratios in magmatic environs. Lithos 212–215, 397–414. https://doi.org/10.1016/j.lithos.2014.11.021.

Lains Amaral, J., Ferreira, E., Solá, A.R., Bento dos Santos, T.M., Albardeiro, L., Gonçalves, J., submitted. Zircon separation workflow: methods, techniques and bias - lessons from the volcanic rocks of the Iberian.

Large, R.R., Gemmell, J.B., Paulick, H., Huston, D.L., 2001. The Alteration Box Plot: A Simple Approach to Understanding the Relationship between Alteration Mineralogy and Lithogeochemistry Associated with Volcanic-Hosted Massive Sulfide Deposits. Econ. Geol. 96, 957–971. https://doi.org/10.2113/gsecongeo.96.5.957.

Leat, P.T., Jackson, S.E., Thorpe, R.S., Stillman, C.J., 1986. Geochemistry of bimodal basalt-subalkaline/peralkaline rhyolite provinces within the Southern British Caledonides. J. Geol. Soc. London 143, 259–273. https://doi.org/10.1144/gsjgs.143.2.0259.

Leistel, J.M., Marcoux, E., Thiéblemont, D., Quesada, C., Sánchez, A., Almodóvar, G.R., Pascual, E., Sáez, R., 1997. The volcanic-hosted massive sulphide deposits of the Iberian Pyrite Belt. Miner. Depos. 33, 2–30. https://doi.org/10.1007/s001260050130.

Leitão, J.C., 2009. Geodinâmica varisca, vulcano-sedimentar e tectónica, na área de Aljustrel. Unpublished PhD. Universidade de Trás-os-Montes e Alto Douro, Portugal, p. 448.

Li, X., Zhao, K.-D., Jiang, S.-Y., Palmer, M.R., 2019. In-situ U-Pb geochronology and sulfur isotopes constrain the metallogenesis of the giant Neves Corvo deposit, Iberian Pyrite Belt. Ore Geol. Rev. 105, 223–235. https://doi.org/10.1016/J.OREGEOREV.2018.12.023.

Ludwig, K.R., 2012. User's manual for Isoplot 3.75, a geochronological toolkit for Microsoft Excel., Berkeley Geochronology Center Special Publication No. 5.

Ludwig, K.R., 2009. SQUID 2: a user's manual. Berkeley Geochronol. Cent. Spec. Publ. 5, 110.

Marques, A.F.A., Relvas, J.M.R.S., Scott, S.D., Rosa, C., Guillong, M., 2020. Melt inclusions in quartz from felsic volcanic rocks of the Iberian Pyrite Belt: Clues for

magmatic ore metal transfer towards VMS-forming systems. Ore Geol. Rev. 126 https://doi.org/10.1016/j.oregeorev.2020.103743.
Mathur, R., Ruiz, J., Tornos, F., 1999. Age and sources of the ore at Tharsis and Rio Tinto, Iberian Pyrite Belt, from Re-Os isotopes. Miner. Depos. 34, 790–793. https://doi.org/10.1007/s001260050239.
Matos, J.X., Pereira, Z., Fernandes, P., Rosa, D.R.N., Oliveira, J.T., 2010. Contribuição para o estudo da estrutura da mina de Aljustrel, Faixa Piritosa Ibérica, com base em novos dados palinoestratigráficos do Complexo Vulcano-Sedimentar e da Fm, Mértola. In: VIII Congresso Nacional de Geologia, pp. 1–4.
Mello, C.R.D., 2020. Estudo isotópico de U-Pb, Lu-Hf e Ti em rochas vulcânicas associadas aos sulfetos maciços da Faixa Piritosa Ibérica (Espanha). Unpublished PhD. Universidade de São Paulo, Brazil, p. 285.
Mendes, M., Pereira, Z., Matos, J.X., Albardeiro, L., Morais, I., Solá, R., Salgueiro, R., Pacheco, N., Araújo, V., Inverno, C., Oliveira, J.T., 2020. New insights on the middle Givetian/middle Frasnian palynofloras from the Phyllite-Quartzite Formation in the Neves-Corvo mine region (Iberian Pyrite Belt, Portugal). Rev. Micropaléontologie 68. https://doi.org/10.1016/j.revmic.2020.100447.
Mudd, G.M., Jowitt, S.M., Werner, T.T., 2017. The world's lead-zinc mineral resources: Scarcity, data, issues and opportunities. Ore Geol. Rev. 80, 1160–1190. https://doi.org/10.1016/j.oregeorev.2016.08.010.
Munhá, J., 1990. Metamorphic Evolution of the South Portuguese/Pulo Do Lobo Zone. In: Dallmeyer, R.D., Garcia, E.M. (Eds.), Pre-Mesozoic Geology of Iberia. Springer, Berlin Heidelberg, pp. 363–368. https://doi.org/10.1007/978-3-642-83980-1_25.
Munhá, J., Relvas, J.M.R.S., Barriga, F.J.A.S., Conceição, P., Jorge, R.C.G.S., Mathur, R., Ruiz, J., Tassinari, C.C.G., 2005. Osmium isotope systematics in the Iberian Pyrite Belt. In: Mineral Deposit Research: Meeting the Global Challenge. Springer, Berlin Heidelberg, pp. 663–666. https://doi.org/10.1007/3-540-27946-6_169.
Nesbitt, R.W., Pascual, E., Fanning, C.M., Toscano, M., Sáez, R., Almodóvar, G.R., 1999. U-Pb dating of stockwork zircons from the eastern Iberian Pyrite Belt. J. Geol.Soc. London 156, 7–10. https://doi.org/10.1144/gsjgs.156.1.0007.
Nieto, J.M., Almodóvar, G.R., Pascual, E., Sáez, R., Jagoutz, E., 1999. Estudio isotópico con el sistema Re-Os de las mineralizaciones de sulfuros de la Faja Pirítica Ibérica. Geogaceta 27, 127–129.
Oliveira, J.T., 1990. Stratigraphy and Synsedimentary Tectonism. In: Dallmeyer, R.D., Garcia, E.M. (Eds.), Pre-Mesozoic Geology of Iberia. Springer, Berlin Heidelberg, pp. 334–347. https://doi.org/10.1007/978-3-642-83980-1_23.
Oliveira, J.T., Pereira, Z., Carvalho, P., Pacheco, N., Korn, D., 2004. Stratigraphy of the tectonically imbricated lithological succession of the Neves Corvo mine area, Iberian Pyrite Belt, Portugal. Miner. Depos. 39, 422–436. https://doi.org/10.1007/s00126-004-0415-2.
Oliveira, J.T., Pereira, Z., Matos, J.X., Fernades, P., 2009. Investigação Palinostratigráfica da Região da Mina de Aljustrel. Unpublished LNEG Report for Eurozinc, pp. 12.
Oliveira, J.T., Quesada, C., Pereira, Z., Matos, J.X., Solá, A.R., Rosa, D., Albardeiro, L., Díez-Montes, A., Morais, I., Inverno, C., Rosa, C., Relvas, J., 2019. In: South Portuguese Terrane: A Continental Affinity Exotic Unit. Springer, Cham, pp. 173–206.
Oliveira, J.T., Rosa, C.J.P., Pereira, Z., Rosa, D.R.N., Matos, J.X., Inverno, C.M.C., Andersen, T., 2013. Geology of the Rosário-Neves Corvo antiform, Iberian Pyrite Belt, Portugal: new insights from physical volcanology, palynostratigraphy and isotope geochronology studies. Miner. Depos. 48, 749–766. https://doi.org/10.1007/s00126-012-0453-0.
Palomeras, I., Carbonell, R., Ayarza, P., Fernàndez, M., Simancas, J.F., Poyatos, D.M., González Lodeiro, F., Pérez-Estaún, A., 2011. Geophysical model of the lithosphere across the Variscan Belt of SW-Iberia: Multidisciplinary assessment. Tectonophysics. https://doi.org/10.1016/j.tecto.2010.07.010.
Paslawski, L.E., Braid, J.A., Quesada, C., McFarlane, C.M., 2020. Geochronology of the Iberian Pyrite Belt and the Sierra Norte Batholith: Lower Plate Magmatism during Supercontinent Amalgamation? SP503-2020–5 Geol. Soc. London, Spec. Publ. 503. https://doi.org/10.1144/SP503-2020-5.
Pereira, M.F., Chichorro, M., Johnston, S.T., Gutiérrez-Alonso, G., Silva, J.B., Linnemann, U., Hofmann, M., Drost, K., 2012. The missing Rheic Ocean magmatic arcs: Provenance analysis of Late Paleozoic sedimentary clastic rocks of SW Iberia. Gondwana Res. 22, 882–891. https://doi.org/10.1016/j.gr.2012.03.010.
Pereira, Z., Fernandes, P., Matos, J.X., Jorge, R.C.G.S., Oliveira, J.T., 2018. Stratigraphy of the Northern Pulo do Lobo Domain, SW Iberia Variscides: A palynological contribution. Geobios 51, 491–506. https://doi.org/10.1016/j.geobios.2018.04.001.
Pereira, Z., Matos, J.X., Batista, M.J., Solá, A.R., Salgueiro, R., Oliveira, D., Oliveira, J.T., Rosa, C., 2014. "IPB Vectors - Caracterização geológica, estratigráfica e litogeoquímica das unidades geológicas da zona do Algaré, antiforma do Rosário e da mineralização de sulfuretos maciços da Semblana." Unpublished LNEG report for AGC Minas de Portugal. pp. 150.
Pérez-Cáceres, I., Martínez Poyatos, D., Simancas, J.F., Azor, A., 2017. Testing the Avalonian affinity of the South Portuguese Zone and the Neoproterozoic evolution of SW Iberia through detrital zircon populations. Gondwana Res. 42, 177–192. https://doi.org/10.1016/J.GR.2016.10.010.
Peterman, E.M., Reddy, S.M., Saxey, D.W., Snoeyenbos, D.R., Rickard, W.D.A., Fougerouse, D., Kylander-Clark, A.R.C., 2016. Nanogeochronology of discordant zircon measured by atom probe microscopy of Pb-enriched dislocation loops. Sci. Adv. 2, e1601318 https://doi.org/10.1126/sciadv.1601318.
Relvas, J.M., Tassinari, C.C., Munhá, J., Barriga, F.J., 2001. Multiple sources for ore-forming fluids in the Neves Corvo VHMS Deposit of the Iberian Pyrite Belt (Portugal): strontium, neodymium and lead isotope evidence. Miner. Depos. 36, 416–427. https://doi.org/10.1007/s001260100168.
Relvas, J.M.R.S., Barriga, F., Carvalho, J.R.S., Pinto, Á.M.M., Matos, J.X., Rosa, C.J.P., Pereira, Z., 2011. Structure, stratigraphy and hydrothermal alteration at the Gavião orebodies, Aljustrel: reconstruction of a dismembered ore-forming system at the Iberian Pyrite Belt and implications for exploration. In: 11th SGA Biennial Meeting: Let's Talk Ore Deposits. pp. 772–774.
Ribeiro, M.L., Reche, J., López-Carmona, A., Aguilar, C., Bento dos Santos, T., Chichorro, M., Dias da Silva, Í., Díez-Montes, A., González-Clavijo, E., Gutiérrez-Alonso, G., Leal, N., Liesa, M., Martínez, F.J., Mateus, A., Mendes, M.H., Moita, P., Pedro, J., Quesada, C., Santos, J.F., Solá, A.R., Valverde-Vaquero, P., 2019. Variscan Metamorphism. In: Quesada, Cecilio, Oliveira, J.T. (Eds.), The Geology of Iberia: A Geodynamic Approach: Volume 2: The Variscan Cycle. Springer International Publishing, Cham, pp. 431–495. https://doi.org/10.1007/978-3-030-10519-8_12.
Rodrigues, B., Chew, D.M., Jorge, R.C.G.S., Fernandes, P., Veiga-Pires, C., Oliveira, J.T., 2015. Detrital zircon geochronology of the Carboniferous Baixo Alentejo Flysch Group (South Portugal); constraints on the provenance and geodynamic evolution of the South Portuguese Zone. J. Geol. Soc. London 172, 294–308. https://doi.org/10.1144/jgs2013-084.
Rodríguez, N., Díaz-Alvarado, J., Fernández, C., Fuentes, P., Breitkreuz, C., Tassinari, C. C.G., 2019. The significance of U-Pb zircon ages in zoned plutons: the case of the Flamenco pluton, Coastal Range batholith, northern Chile. Geosci. Front. 10, 1073–1099. https://doi.org/10.1016/J.GSF.2018.06.003.
Rosa, D.R.N., Finch, A.A., Andersen, T., Inverno, C.M.C., 2009. U-Pb geochronology and Hf isotope ratios of magmatic zircons from the Iberian Pyrite Belt. Mineral. Petrol. 95, 47–69. https://doi.org/10.1007/s00710-008-0022-5.
Rosa, D.R.N., Finch, A.A., Andersen, T., Inverno, C.M.C., 2008. U-Pb geochronology of felsic volcanic rocks hosted in the Gafo Formation, South Portuguese Zone: the relationship with Iberian Pyrite Belt magmatism. Mineral. Mag. https://doi.org/10.1180/minmag.2008.072.5.1103.
Rossignol, C., Hallot, E., Bourquin, S., Poujol, M., Jolivet, M., Pellenard, P., Ducassou, C., Nalpas, T., Heilbronn, G., Yu, J., Dabard, M.-P., 2019. Using volcaniclastic rocks to constrain sedimentation ages: To what extent are volcanism and sedimentation synchronous? Sediment. Geol. 381, 46–64. https://doi.org/10.1016/J.SEDGEO.2018.12.010.
Sato, K., Tassinari, C.C.G., Basei, M.A.S., Júnior, O.S., Onoe, A.T., de Souza, M.D., 2014. Microssonda Iônica de Alta Resolução e de Alta Sensibilidade (SHRIMP IIe/MC) do Instituto de Geociências da Universidade de São Paulo, Brasil: método analítico e primeiros resultados, Geol. USP. Série Científica 14, 3–18.
Schermerhorn, L.J.G., 1971. An outline stratigraphy of the Iberian Pyrite Belt. Boletín Geológico y Min. 82, 239–268.
Schermerhorn, L.J.G., Zbyszewski, G., Ferreira, O., 1987. Carta Geologica de Portugal 1: 50 000. Noticia Explicativa da Folha 42-D (Aljustrel). Serviços Geológicos Port.
Schmelzbach, C., Simancas, J.F., Juhlin, C., Carbonell, R., 2008. Seismic reflection imaging over the South Portuguese Zone fold-and-thrust belt, SW Iberia. J. Geophys. Res. Solid Earth 113, B08301. https://doi.org/10.1029/2007JB005341.
Sieck, P., López-Doncel, R., Dávila-Harris, P., Aguillón-Robles, A., Wemmer, K., Maury, R.C., 2019. Almandine garnet-bearing rhyolites associated to bimodal volcanism in the Mesa Central of Mexico: Geochemical, petrological and geochronological evolution. J. South Am. Earth Sci. 92, 310–328. https://doi.org/10.1016/j.jsames.2019.03.018.
Siégel, C., Bryan, S.E., Allen, C.M., Gust, D.A., 2018. Use and abuse of zircon-based thermometers: a critical review and a recommended approach to identify antecrystic zircons. Earth-Science Rev. 176, 87–116. https://doi.org/10.1016/j.earscirev.2017.08.011.
Silva, J.B., Oliveira, J.M., Matos, J., Leitão, J.C., 1997. Aljustrel and the Central Iberian Pyrite Belt. In: Geology and VMS Deposits of the Iberian Pyrite Belt, SEG Neves Corvo Field Conference. pp. 73–12.
Simancas, J.F., Carbonell F. González Lodeiro, R., Pérez Estaún, A., Juhlin, C., Ayarza, P., Kashubin, A., Azor, A., Martínez Poyatos, D., Almodóvar, G.R., Pascual, E., Sáez, R., Expósito, I., 2003. Crustal structure of the transpressional Variscan orogen of SW Iberia: SW Iberia deep seismic reflection profile (IBERSEIS). Tectonics 22, 1062. https://doi.org/10.1029/2002TC001479.
Solá, A.R., Salgueiro, R., Pereira, Z., Matos, J.X., Rosa, C., Araújo, V., Neto, R., Lains, J. A., 2015. Time span of the volcanic setting of the Neves-Corvo VHMS deposit. In: X Congresso Ibérico de Geoquímica : XVIII Semana de Geoquímica. Laboratório Nacional de Energia e Geologia, pp. 122–125.
Spencer, C.J., Kirkland, C.L., Taylor, R.J.M., 2016. Strategies towards statistically robust interpretations of in situ U-Pb zircon geochronology. Geosci. Front. 7, 581–589. https://doi.org/10.1016/J.GSF.2015.11.006.
Stacey, J.S., Kramers, J.D., 1975. Approximation of terrestrial lead isotope evolution by a two-stage model. Earth Planet. Sci. Lett. 26, 207–221.
Tichomirowa, M., Käßner, A., Sperner, B., Lapp, M., Leonhardt, D., Linnemann, U., Münker, C., Ovtcharova, M., Pfänder, J.A., Schaltegger, U., Sergeev, S., von Quadt, A., Whitehouse, M., 2019. Dating multiply overprinted granites: The effect of protracted magmatism and fluid flow on dating systems (zircon U-Pb: SHRIMP/SIMS, LA-ICP-MS, CA-ID-TIMS; and Rb–Sr, Ar–Ar) – Granites from the Western Erzgebirge (Bohemian Massif, Germany). Chem. Geol. 519, 11–38. https://doi.org/10.1016/J.CHEMGEO.2019.04.024.
Tornos, F., 2006. Environment of formation and styles of volcanogenic massive sulfides: The Iberian Pyrite Belt. Ore Geol. Rev. 28, 259–307. https://doi.org/10.1016/J.OREGEOREV.2004.12.005.
Valenzuela, A., Donaire, T., Pin, C., Toscano, M., Hamilton, M.A., Pascual, E., 2011. Geochemistry and U-Pb dating of felsic volcanic rocks in the Riotinto-Nerva unit, Iberian Pyrite Belt, Spain: crustal thinning, progressive crustal melting and massive sulphide genesis. J. Geol. Soc. London 168, 717–732. https://doi.org/10.1144/0016-76492010-081.
Valley, J.W., Cavosie, A.J., Ushikubo, T., Reinhard, D.A., Lawrence, D.F., Larson, D.J., Clifton, P.H., Kelly, T.F., Wilde, S.A., Moser, D.E., Spicuzza, M.J., 2014. Hadean age

for a post-magma-ocean zircon confirmed by atom-probe tomography. Nat. Geosci. 7, 219–223. https://doi.org/10.1038/ngeo2075.
Wang, X., Griffin, W.L., Jie, C., Pinyun, H., Xiang, L.I., 2011. U and Th contents and Th/U ratios of zircon in felsic and mafic magmatic rocks: improved zircon-melt distribution coefficients. Acta Geol. Sin. - English Ed. 85, 164–174. https://doi.org/10.1111/j.1755-6724.2011.00387.x.
Williams, I.S., 1998. U-Th-Pb geochronology by ion microprobe. Rev. Econ. Geol. 7, 1–35.
Winchester, J.A., Floyd, P.A., 1977. Geochemical discrimination of different magma series and their differentiation products using immobile elements. Chem. Geol. 20, 325–343. https://doi.org/10.1016/0009-2541(77)90057-2.
Xu, X.-S., Zhang, M., Zhu, K.-Y., Chen, X.-M., He, Z.-Y., 2012. Reverse age zonation of zircon formed by metamictisation and hydrothermal fluid leaching. Lithos 150, 256–267. https://doi.org/10.1016/j.lithos.2011.12.014.